



THE UNIVERSITY *of*  
**MISSISSIPPI**



MDOT State Study 319

# Seismic Bearing Selection for Economic Prestressed Concrete Bridge Pier Construction

---

Chris L. Mullen\*, Ph.D. and Elizabeth K. Ervin\*, Ph.D.

\* Associate Professor of Civil Engineering  
University of Mississippi

Report Date: 06/30/2022

**Final Report**

**FHWA Technical Report Documentation Page**

<b>1. Report No.</b>  FHWA/MDOT-RD-FY-2022-319	<b>2. Government Accession No.</b>	<b>3. Recipient's Catalog No.</b>
<b>4. Title and Subtitle</b> Seismic Bearing Selection for Economic Prestressed Concrete Bridge Pier Construction	<b>5. Report Date</b> 06-30-2022	<b>6. Performing Organization Code</b>
	<b>7. Author(s)</b> Chris Mullen, <a href="https://orcid.org/0000-0003-0081-0284">https://orcid.org/0000-0003-0081-0284</a> Elizabeth Ervin, <a href="https://orcid.org/0000-0002-5014-4585">https://orcid.org/0000-0002-5014-4585</a>	<b>8. Performing Organization Report No.</b> State Study # 319
<b>9. Performing Organization Name and Address</b> University of Mississippi PO Box 1848 University, MS 38677-1848	<b>10. Work Unit No. (TR AIS)</b>	
	<b>11. Contract or Grant No.</b> MSU Subaward 060502.303951.01	
<b>12. Sponsoring Agency Name and Address</b> Mississippi Department of Transportation PO Box 1850 Jackson, MS 39215-1850	<b>13. Type Report and Period Covered</b> July 1, 2021 to June 30, 2022	
	<b>14. Sponsoring Agency Code</b>	
<b>15. Supplementary Notes</b>		
<b>16. Abstract</b>  In this review of seismic bearings, a compendium of public domain resources provides off-the-shelf, state-of-the-art bearing types, manufacturers, researchers, and load-deformation response data. Performance of two select seismic bearings, one generally available and one proprietary, is then assessed using finite element modeling and simulation. The influence of seismic bearing effective stiffness is evaluated in terms of reduction of peak in-plane bending moments computed in critical elements of select multi-column pier and trestle substructures used in highway bridges in north Mississippi for a simulated scenario earthquake event.  Modeling is performed primarily using frame elements for the steel and reinforced concrete substructures components. Linear springs are used to represent the action of the shearing response of the bearings and the soil resistance. Vertical and lateral stiffness of the springs is established from the literature review using results of a comparative experimental study that presents load-deformation response of the select seismic bearings. Input motion is applied as an acceleration time history whose intensity has been scaled to match findings reported in a prior study that has guided development of emergency management plans for the state. Deck inertial effects are developed through point masses located at the centers of gravity of the concrete deck slab and girders using elements that mimic the girder transverse stiffening system. Two-column pier cases are developed based on the design drawings provided for		

intermediate bents 7 (steel girders) and 9 (prestressed concrete girders) of the existing MS 7 bridge over the Tallahatchie River. A trestle case is developed based on the design drawings provided for intermediate bent 5 of the replacement of the existing US51 bridge over Long Creek. Supplemental nonlinear pushover and solid modeling analyses have been performed to provide context of the linear frame response analyses.

The compendium created from the literature review lists 20 companies, 22 published articles, and 22 universities involved in relevant research. The most significant study relevant to the objectives of the present one proved to be a study jointly sponsored by a reputable university in Korea and a global structural engineering firm specializing in large bridges. Load-deformation plots from this study enable the estimation of spring constants used in the finite element modeling.

The modeling and simulation provide a wealth of in-plane lateral response behavior, but the study focuses on comparison of the maximum internal flexural responses computed in critical column, shaft, and pile sections. Performance of the bearings is then quantified in terms of demand-capacity ratios. The simulations indicate the select seismic bearings provide significant benefits relative to the non-seismic case in terms of reduce demand at the critical column section of the select two-column pier cases. Little benefit is observed however for the shafts of the select two-column pier cases and the piles of the trestle case. The simulation results do not account for nonlinear response directly or for substructure interaction seen in full bridge response. These effects will be considered in an ongoing study.

Based upon the potential 20-30 % reductions in flexural demands in the columns of the two-column piers studied, it is recommended that seismic bearing modeling be implemented in future analyses performed by MDOT during the design sensitivity stage of future projects to develop a more robust cost-benefit evaluation.

<b>17. Key Words</b> Safety, economic benefits, base isolation, bridge bearing pads, substructure, finite element method		<b>18. Distribution Statement</b> Unclassified	
<b>19. Security Classif. (of this report)</b> Unclassified	<b>20. Security Classif. (of this page)</b> Unclassified	<b>21. No. of Pages</b>	<b>22. Price</b>

## **Disclaimer**

The University of Mississippi and the Mississippi Department of Transportation do not endorse service providers, products, or manufacturers. Trade names or manufacturers' names appear herein solely because they are considered essential to the purpose of this report.

The contents of this report do not necessarily reflect the views and policies of the sponsor agency.

## **MDOT Statement of Nondiscrimination**

The Mississippi Department of Transportation (MDOT) operates its programs and services without regard to race, color, national origin, sex, age or disability in accordance with Title VI of the Civil Rights Act of 1964, as amended and related statutes and implementing authorities.

## **Mission Statements**

### **The Mississippi Department of Transportation (MDOT)**

MDOT is responsible for providing a safe intermodal transportation network that is planned, designed, constructed and maintained in an effective, cost efficient and environmentally sensitive manner.

### **The Research Division**

MDOT Research Division supports MDOT's mission by administering Mississippi's State Planning and Research (SP&R) Part II funds in an innovative, ethical, accountable, and efficient manner, including selecting and monitoring research projects that solve agency problems, move MDOT forward, and improve the network for the traveling public.

## **Author Acknowledgments**

The authors would like to thank the Mississippi Department of Transportation, Research and Bridge Divisions, for the sponsorship of direction of this work. The project management assistance of Ms. Cynthia Smith and technical guidance of Mr. Scott Westerfield and the cooperation of the Mississippi Department of Transportation, Bridge Division in providing PDF files containing design drawings for the select bridge cases is greatly appreciated.

The FE modeling and simulation performed in the project could not have been completed without the dedicated and competent work performed by Mr. Sandip Gupta, recent graduate from the University of Mississippi Civil Engineering undergraduate program and an entering student in the masters program, and by Mr. Othman Hama Rahim, currently a graduate student in the University of Mississippi Mechanical Engineering doctoral program. These two research assistants worked effectively as a team sharing information and lessons learned. Mr. Gupta was responsible for interpreting design drawing data for the deck loading and obtaining simulation results using SAP2000. Mr. Hama Rahim was responsible for preparing 3D solid geometry definition using AutoCAD and obtaining simulation results using Abaqus CAE.

# Contents

Disclaimer..... iv

MDOT Statement of Nondiscrimination ..... v

Mission Statements ..... v

    The Mississippi Department of Transportation (MDOT) ..... v

    The Research Division ..... v

Author Acknowledgments ..... vi

List of Figures and Tables ..... viii

List of Abbreviations ..... ix

Executive Summary..... x

Introduction/Background ..... 1

Seismic Bearing Literature Review..... 3

FE Substructure Modeling and Simulation ..... 8

FE Analysis Results ..... 15

Conclusions ..... 25

Implementation Plan/Recommendations..... 28

References ..... 30

Appendix A Compendium of Seismic Bearing Literature..... 31

Appendix B MDOT Design Drawings ..... 35

Appendix C FE Software Descriptions and Menu Screen Captures ..... 50

## List of Figures

Figure 1. Example of lateral compression-shear test literature. Seismic Isolation Bearing Systems Brochure, D. S. Brown, <a href="https://www.dsbrown.com/wp-content/uploads/2020/12/B_Seismic_Bro_v005-1.pdf">https://www.dsbrown.com/wp-content/uploads/2020/12/B_Seismic_Bro_v005-1.pdf</a> (Accessed 6/4/2022).....	4
Figure 2. Bearing effective linear and bilinear stiffness definitions [1] (left) and bilinear hysteresis plots obtained by digitizing experimental results of the comparative study [9] (right).....	7
Figure 3. Substructure model developed using FE-based structural software [10] (left) and general-purpose software [11] (right).....	10
Figure 4. Graphical estimate of $K_{eff}$ used to define Line Spring properties for NRB (top), LRB (mid), and EQS (bot) cases using data from comparative experimental study [9].....	11
Figure 5. Idealized soil profiles for the two-column pier (left) and trestle (right) bridge locations used in the FE modeling. ....	12
Figure 6. Input time history acceleration used for the study based on prior studies [5], [6], [8] .....	14
Figure 7. Characteristic lateral mode shape computed for RGD cases for MS7 IB7 (left), MS7 IB9 (middle), US51 IB5 (right) (deformation scale and direction are arbitrary).....	16
Figure 8. Comparison of lateral mode shape computed for the NRB case for MS7 IB7 (left), MS7 IB9 (middle), and US51 IB5 (right) (deformation scale and direction are arbitrary) .....	17
Figure 9. Comparison of deformed shapes at time of peak computed bending moment for the MS7 IB7 RGD (left), MS7 IB9 EQS (middle), and US51 IB5 NRB (right) cases.....	19
Figure 10. Comparison of bending moment diagrams computed for the MS7 IB7 RGD (left), MS7 IB9 EQS (middle), and US51 IB5 NRB (right) cases .....	20
Figure 11. Typical computed bending moment (M3) time history (MS7 IB9 EQS case, k-ft) .....	21
Figure 12. Geometry for substructure as created in 3D drawing tool (top left and right) and as imported into solid modeling FE tool (bottom).....	23
Figure 13. Bending stress distribution in concrete substructure elements (top and middle) and in embedded steel reinforcement (bottom) calculated by FE tool for unit later load case.....	24

## List of Tables

Table 1. Important values from digitized results from Korean study. ....	7
Table 2. Soil spring stiffness estimates using the equivalent circular footing on a half space approach applied in a prior UM study of seismic vulnerability of north MS bridges [5].....	12
Table 3. Bearing dead load estimates.....	13
Table 4. Estimates of bent lateral stiffness and effective SDOF frequency for RGD bearing case. ....	15
Table 5. Computed natural period and frequency for characteristic lateral mode RGD cases. ....	16
Table 6. Computed frequencies for characteristic modes for all bent and bearing cases. ....	18
Table 7. Comparison of peak bending moments computed for the pier and trestle cases. ....	21



## List of Abbreviations

<i>EQS</i>	EradiQuake System by R.J. Watson, Inc.
<i>FE</i>	Finite Element
<i>FEMA</i>	Federal Emergency Management Agency
<i>HDRI</i>	High Damping Rubber Isolator
<i>HPC</i>	High Performance Computing
<i>IB</i>	Intermediate Bent
<i>LRB</i>	Lead Rubber Bearing
<i>MS</i>	Mississippi
<i>MDOT</i>	Mississippi Department of Transportation
<i>MAEC</i>	Mid-America Earthquake Center
<i>MEMA</i>	Mississippi Emergency Management Agency
<i>MER</i>	Mass Energy Regulator springs in EQS by R.J. Watson, Inc.
<i>NMFZ</i>	New Madrid Fault Zone
<i>NRB</i>	Natural Rubber Bearing
<i>RGD</i>	Rigid bearing connection
<i>UM</i>	University of Mississippi
$\nu$	Poisson's ratio
$\delta_{max}$	Maximum shear displacement, <i>in</i>
$D_{max}$	Maximum shear displacement, <i>in</i>
$E$	Young's modulus, <i>ksi</i>
$F_{max}$	Maximum lateral load, <i>k</i>
$K_d$	Post-elastic stiffness, <i>k/in</i>
$K_{eff}$	Effective bearing stiffness, <i>k/in</i>
$K_u$	Elastic stiffness, <i>k/in<sup>2</sup></i>
$M$	Bending moment, <i>k · ft</i>
$P$	Axial force, <i>k</i>
$P_{max}$	Maximum vertical load, <i>k</i>
$PGA$	Peak ground acceleration, % <i>g</i>
$Q_d$	Characteristic load, <i>k</i>

## Executive Summary

An investigation by the Structural Systems group of the University of Mississippi Department of Civil Engineering has been conducted to identify the potential effectiveness of seismic bearings in reducing forces developed in typical highway bridge substructure types in use by MDOT. An extensive research literature and manufacturing vendor review of major bearing types currently in use has been conducted to develop a compendium of citations for future reference by MDOT, and detailed finite element (FE) modeling and simulation have been performed for select cases identified by Bridge Division as being of particular interest. The bearing types selected are: 1) a reference non-seismic bearing (i.e. layered neoprene with steel reinforcement of limited height and shear deformation capacity) similar to ones currently in use by MDOT, 2) a widely used seismic bearing (Lead Rubber Bearing or LRB with significant height and shear deformation capacity), and 3) a proprietary seismic bearing (EradiQuake or EQS rubber disc system). Each bearing type has been studied in conjunction with one of two select substructure types currently in use in the region with significant seismic hazard: 1) a two-column pier with foundation shafts, and 2) a trestle with driven steel multi-pile foundation.

An experimental study performed in Korea has been identified that provides quantitative load-deformation response of the three select bearing types considered in the present study. Bearing equivalent stiffness is derived from these results for use in the FE modeling. The SAP2000 FE-based structural software currently in use by Bridge Division has been selected as the most robust and efficient method of performing the system modeling for the various cases. The general purpose Abaqus CAE FE-based solid element modeling software has been used to develop models to benchmark potential benefits of more detailed full-bridge modeling being adopted in a recently initiated study for Bridge Division on improving bridge resilience. SAP2000 system models consist of isolated bents modeled primarily using frame elements subjected to self-weight, deck gravity, and inertial loads. Static, modal, and time history analyses have been performed to assess the response to lateral loading with and without bearings. Nonlinear static analyses are performed to establish failure criteria for the frame elements associated with the presence of internal axial force and bending moment. Input motion for the time history analysis consists of a simulated site-specific acceleration realization developed for a prior seismic vulnerability study UM sponsored by MDOT that has been scaled to match the peak ground acceleration predicted for bridge locations on I-55 in Mississippi near the Tennessee border during a simulated New Madrid M7.7 earthquake scenario event developed by the Mid-America Earthquake Center in a loss-estimation study sponsored by DHS/FEMA for use in developing state emergency management plans.

Time history simulations provide estimates of dynamic response of the substructures, including motion above and below the bearings as well as axial/bending response of the pier and trestle

members, under inertial forces generated by accelerations at the deck and girder center-of-mass elevations. Contributions of the weight and mass of superstructure elements are considered for typical spans over typical spans of the select bridge cases. Locations of maximum axial load and bending moment in the substructure elements are identified from the time history analyses of the scenario event. The section responses in the critical column, shaft, and pile members are compared for each of the bearing cases and the effectiveness in reducing the demand established using demand-capacity ratios as a basis for comparison.

The computed peak moments from the time history simulation indicate the bearings would provide some benefit over non-seismic bearings in reducing the demand on the critical column section of the two-column piers. The benefit of the bearing for the shafts of the two-column pier and the piles of the trestle cases appears minimal owing primarily to the low demand-capacity ratio observed for these cases based on the current design practice. The simulation results do not account for three-dimensional multi-pier/abutment response in full bridge systems which will be considered in a follow-on study. It is recommended that seismic bearing modeling be implemented in at least some analyses performed by MDOT during the design sensitivity stage of future projects to develop a more robust cost-benefit evaluation.

## Introduction/Background

The present study evaluates the potential effectiveness of seismic bearings in reducing forces transmitted to typical multi-column piers and trestles supporting bridge decks in regions of northern Mississippi where the exposure to the earthquake hazard is considered greatest. The overall goal is to assess whether the reductions are significant enough to justify size reductions of critical components of these substructures such as columns, caps, shafts, and piles and thereby achieve cost savings by employing such bearings in future projects located in this region.

The project is an outgrowth of discussions held with staff in the Bridge Division of the Mississippi Department of Transportation (MDOT) in recent years who have expressed the view that current guidelines for seismic design of highway bridges [1, 2] with conventional non-seismic bearings has resulted in the need to implement large substructures that are expensive to construct.

The specific objectives of the study established after consultation with Bridge Division staff are to:

1. Conduct a literature review of off-the-shelf products by suppliers in the United States (US), develop a compendium of candidate seismic bearing systems of potential use by Bridge Division staff, and identify published load-deformation response behavior of select systems under compression and shear for use in structural system modeling and simulation
2. Construct detailed finite element (FE) models of representative isolated multi-column pier and trestle substructure subsystems with and without select seismic bearings, perform static and eigenvalue analyses to calibrate the load-deformation behavior of the subsystems under lateral (in-plane) loading, and simulate response of the subsystems to lateral loading under a time history representative of ground shaking caused by a design level scenario earthquake event.

Details of the seismic bearing product search methodology and literature review are provided in the next section. Issues addressed include a) limitations encountered during the search and review and 2) extraction of load-deformation data for select bearings from a comparative experimental study.

Details of the FE modeling and simulation adopted in the study are provided in the subsequent section. Issues addressed in the FE analysis include the characterization of the: a) superstructure, bearing, substructure, and soil; b) interaction between these subsystems, c) effective superstructure gravity and inertial loading; and d) time history for the scenario earthquake input ground motion.

The literature search methodology was established by the second author based on her research at the University of Mississippi (UM) in the Multi-Functional Dynamics Lab (MFDL) [3,4] and her initial contacts with bearing manufacturers during the project proposal development stage.

The FE analysis methodology was established based on conversations between the first author and Bridge Division modelers and on prior bridge seismic structural response research directed by the first author in a variety of studies at UM sponsored by MDOT Bridge Division [5], Mississippi Emergency Management Agency (MEMA) [6], and the US Department of Transportation (USDOT) [7]. Ground motion simulation for a scenario event has been adapted from a prior study sponsored by MDOT Bridge Division directed by the first author and from more recent research performed by the Mid-America Earthquake Center (MAEC) sponsored by the Department of Homeland Security/Federal Emergency Management Agency (DHS/FEMA) [8].

The compendium of candidate bearing systems is provided in Appendix A as a sequence of lists of manufacturers, journal articles containing related research, and universities performing the research.

Supporting references and data from external sources relevant to the FE modeling and simulation are provided in supplemental appendices. Appendix B contains photos of one of the bridge sites excerpts of MDOT design drawings for the select substructures, and Appendix C contains FE software descriptions and sample screen captures for models depicting key features and data used in the modeling and simulation.

# Seismic Bearing Literature Review

## Review Methodology and Reference List Preparation

The literature review consisted of internet searching, library resources, personal contacts, and email/phone correspondence by the second author. Experimental results in academic publications were examined through the J.D. Williams Library at UM. Input was received from MDOT Bridge Division, and those sources were reviewed. Direct contact was made in numerous cases to request access to test data with differing responses.

Three lists of references developed through the review are provided in Appendix A:

- A1. Manufacturers
- A2. Journal Articles
- A3. Universities

The lists represent a cumulative output of the review, as one source or article led to another reference or manufacturer.

The literature reviewed commonly provided some types of information on seismic isolation bearings. While material properties are the main discussion topic, only specific material values are revealed. Pure compression test results may be presented to verify vertical stiffness values. A reader may also find friction coefficient and temperature discussions.

The literature reviewed rarely provides certain important discussions. Documentation rarely addresses maintenance. Most companies consider their products self-lubricating, and replacement is not mentioned. Additionally, designs often include lateral displacement limiters, which are usually encasement stoppers with their own shear key loads (not discussed). Most importantly, lateral shear stiffness or modulus may be provided, but test data are rarely available. If slip test data are presented by a source, the data likely relate to only one case with a single configuration and load case. For instance, Figure 1 provides a sample excerpt from a typical company publication with a lateral force (kips) versus displacement (inches) plot for a specific bridge case under constant axial compressive load. The plot reveals that in this case, the bearing exhibits specific stiffness slopes  $K_d$  for the resulting actual maximum shear displacement  $D_{max} = 3.5 \text{ in}$  and lateral load range  $F_{max} = +115 \text{ k}/-105 \text{ k}$  under constant vertical load  $P_{max} = 400 \text{ k}$ .

The three lists in Appendix A include the 20 companies, 22 articles, and 22 universities examined in the literature review. The most important contact and extensive study were related to a proprietary bearing, EradiQuake System (EQS), recommended by MDOT Bridge Division. The president and engineers of the company that manufactures the EQS bearing (R. J Watson, Inc., <https://www.rjwatson.com/>, last accessed 6/21/2022) were very responsive and

helpful, providing available data from in-house and partner testing. The company provided material test data for their fixed disk bearings, which are also found in their EQS bearing as a polytetrafluoroethylene (PTFE) disk. Understandably, the company is obligated to protect their

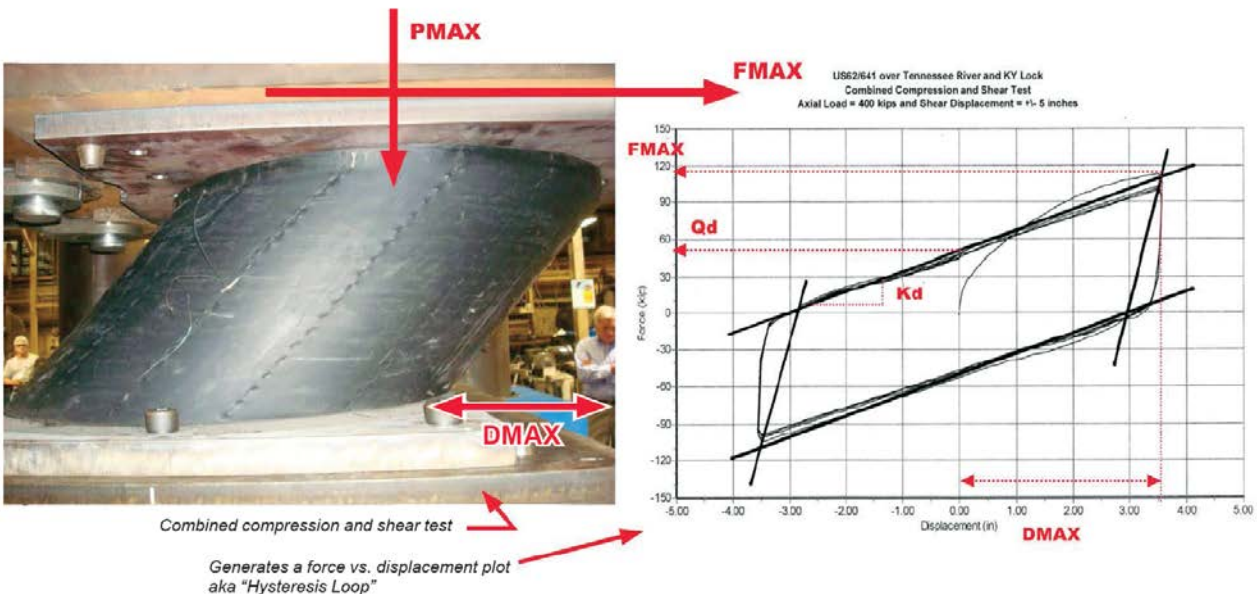


**Figure 1.** Example of lateral compression-shear test literature. Seismic Isolation Bearing Systems Brochure, D. S. Brown, [https://www.dsbrown.com/wp-content/uploads/2020/12/B\\_Seismic\\_Bro\\_v005-1.pdf](https://www.dsbrown.com/wp-content/uploads/2020/12/B_Seismic_Bro_v005-1.pdf) (Accessed 6/4/2022).

proprietary information relating to the other components in the EQS bearing. While the company provided a document on exactly what is typically needed to design an EQS bearing for a specific application, the process is considered a “black box.” For instance, little information is provided on the bearing’s lateral Mass Energy Regulator (MER) springs, which are likely tuned in a proprietary manner; these components also act as displacement limiters, a potentially important aspect of the FE modeling.

Additionally, MDOT Bridge Division has recommended two sources:

- 1) Zaoqiang Dacheng Rubber Co, Ltd., Sino Technology (<https://www.bridgebearing.org/>, last accessed 6/21/2022), a supplier of lead rubber bearings- an excellent test video is available (<https://youtu.be/LTa9g6noUAQ>, last accessed 6/21/2022), but after emailing the company, no data was found to be available
- 2) Bowman Construction Supply, Inc. (<https://www.bowmanconstructionsupply.com/>, last accessed 6/21/2022), an affiliate of D.S. Brown and Company (<https://www.dsbrown.com/>, last accessed 6/21/2022)

## Comparative Experimental Study of Seismic Bearing Load-Deformation Characteristics

Project modeling requires stiffness baselines for use in FE modeling of the bearings under consideration:

1. non-seismic
2. natural rubber bearing (NRB)
3. lead rubber bearing (LRB)
4. proprietary bearing (EQS)

The project budget did not enable purchases of the bearings, however, and equipment available to the investigators at UM would not have allowed testing of large full-scale components. Fortunately, however, the literature search revealed the existence of a comparative experimental study of seismic bearings performed in Korea in 2020 [9].

The experimental study was sponsored by the Korea Institute of Civil Engineering and Building Technology (KICT, considered a reputable university by the second author) and the National Research Foundation of Korea (the counterpart of the US National Science Foundation, NSF). Both KICT and Kyungpook National University participated as well as Teratec (<https://www.teratec.ca/>, last accessed 6/21/2022), a global structural engineering firm specializing in large bridge structures. The goal of the study was to test seismic apparatus for isolation in bridge systems with an “economic and practical strategy.”

The most significant result of this project and its publication is a direct comparison of typical NRB, analogous LRB, and proprietary EQS bearing deformation response under load. The authors performed in-house compressive tests and compressive-shear tests, and the paper presents their experimental data. The range of loading and deformation will be seen to encompass the practical limits for bridges being studied in this project. The authors also state that seismic isolation reduces forces and displacements by up to 75% thereby reducing the required foundation size, a conclusion driving the primary goal of this study. It should be noted, however, that based on higher loads applied and deformation limits allowed, the experimental study appears to have targeted longer span bridges than the ones being studied in this project.

The authors of the comparative study conclude that:

1. NRB has the lowest vertical stiffness (1226 kN/mm versus ~1375 kN/mm, 7,000 kips/inch versus ~7,851 kips/inch), was most consistent, absorbed the least energy, and met design criteria (only one)
2. EQS has high shear stiffness (2.74 kN/mm versus 0.97 to 1.31 kN/mm, 15.65 kips/inch versus 5.52 to 7.46 kips/inch) and can resist greater vertical load, but permanent deformation occurred when applied



The authors of the comparative study recommend use of the EQS, as it can easily be fixed after an earthquake, but installation concerns could render the NRB a better choice.

In the comparative study, seven specimens (3 NRB, 3 LRB, and 1 EQS) were tested in both pure compression and compression-shear manners. Similar bridge design parameters were used for ordering the specimens. The NRB and LRB employed the same vertical load of 2945 kN (662.1 kips), the same diameter of 500mm (19.69 inch), and same shear modulus. The design vertical stiffness was 1680 kN/mm (9,592 kips/inch) and 1995 kN/mm (11,391 kips/inch) for the NRB and LRB, respectively. The EQS employed the vertical load of 2775 kN (623.8 kips), a maximum travel of 50mm (1.97 inch), and a diameter of 305mm (12.01 inch). Note that the test results are limited to these specimen designs. It should be noted however that the loads applied in the testing were less in general than the design values and the displacement limits exceeded the design values in some cases.

The test protocol enabled creation of cyclic force versus displacement hysteresis plots. The pure compression test was generated as biaxial loading using two hydraulic actuators. Displacement was measured by linear variable displacement transducers (LVDTs). The vertical design load of 2000 kN (449.6 kips) was used for the NRB and LRB, while 1850 kN (415.9 kips) was employed for the EQS. Specimens were tested over three cycles at 70% to 130% of the design load. The compressive-shear test was performed on a rather complex KICT-designed apparatus. A constant vertical load was maintained, and then the shear force and horizontal displacement were measured. The forces were measured by load cell, which must consider friction despite bearings. Six cycles of loading were performed for hysteresis: the cycle time and amplitude were approximately 200 milliseconds and +100/-100mm (3.94 inch) for NRB and LRB, respectively. The cycle time and amplitude were approximately 100 milliseconds and +50/-50mm (1.97 inch) for the EQS.

The comparative study experimental results are employed herein to extract effective stiffnesses for the non-seismic, LRB, and EQS bearing cases. Data points have been extracted from the published Force (kN) versus Displacement (mm) hysteresis curves. The published curves have been digitized, and average values found for effective bilinear plot locations of characteristic strength, yield force, maximum force, and maximum bearing displacement. Relevant slopes have then been calculated to determine effective stiffness, elastic stiffness, and post-elastic stiffness as defined in US seismic design guidelines [1].

Figure 2 and Table 1 present results of the digitization process. In summary, the lateral compressive-shear test resulted in a displacement of +/- 100mm (3.94 inch) for average forces of +96/-97 kN (+21.58/-21.81 kips) for the NRB case. The same test resulted in a displacement of +/- 100mm (3.94 inch) for greater average forces of +142/-150 kN (+31.92/-33.72 kips) for

the LRB case. Lastly, the shear test resulted in a displacement of +/- 50mm (1.97 inch) for average forces of +132/-142 kN (+29.67/-31.92 kips) for the EQS case.

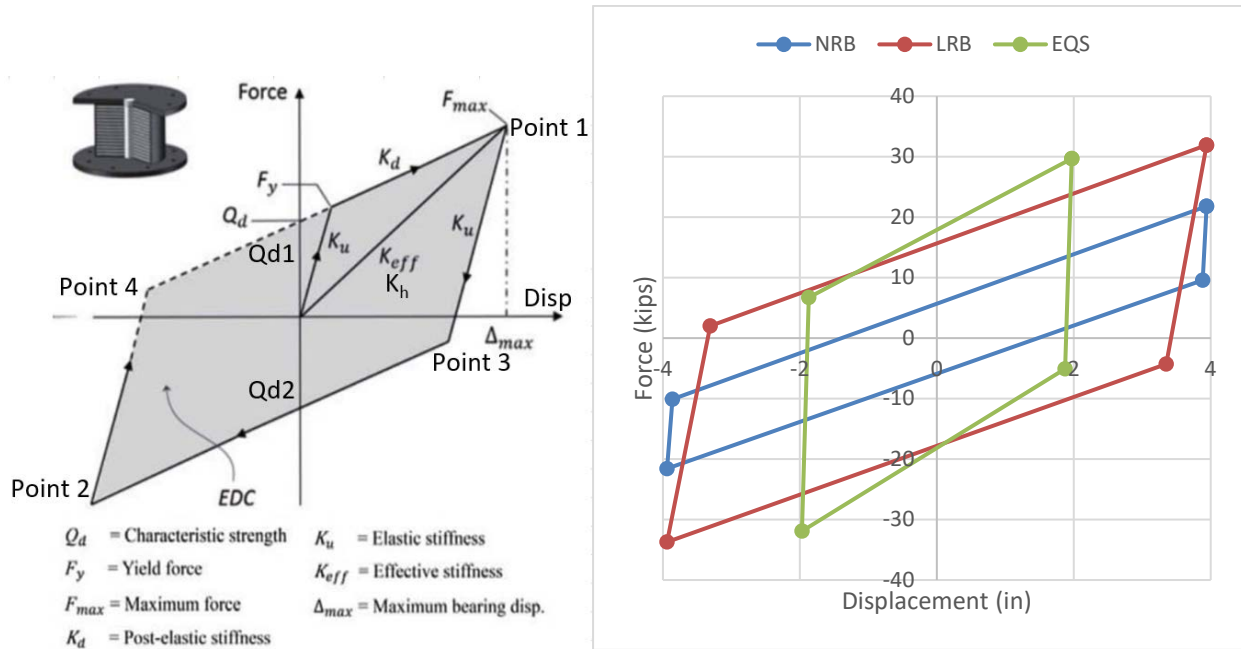


**Figure 2.** Bearing effective linear and bilinear stiffness definitions [1] (left) and bilinear hysteresis plots obtained by digitizing experimental results of the comparative study [9] (right)

**Table 1.** Important values from digitized results from Korean study.

Metric units (mm, kN): (\* denotes from literature)

Point	1		2		3		4		Force		Stiffness			
	X	Y	X	Y	X	Y	X	Y	$Q_{d1}$	$Q_{d2}$	$K_d$	$K_h$	$K_{eff}$	$K_u$
NRB	100	97	-100	-96	98.5	42.5	-98	-45	20	-25	0.707	<b>0.967*</b>		~31.5
LRB	100	142	-100	-150	85	-19	-84	9	78	-80	0.716	<b>1.31*</b>	<b>1.46</b>	10.3
EQS	50	132	-50	-142	47.5	-22.5	-47.5	30	68	-73	~1.13	<b>2.74*</b>		65.3

English units (in, k): (\* denotes from literature)

Point	1		2		3		4		Force		Stiffness			
	X	Y	X	Y	X	Y	X	Y	$Q_{d1}$	$Q_{d2}$	$K_d$	$K_h$	$K_{eff}$	$K_u$
NRB	3.94	21.8	-3.94	21.6	3.88	9.55	-3.86	-10.12	4.50	-5.62	4.03	<b>5.52*</b>		~179.7
LRB	3.94	31.9	-3.94	-33.7	3.35	-4.27	-3.31	2.02	17.42	-17.98	4.09	<b>7.46*</b>	<b>8.33</b>	58.8
EQS	1.97	29.7	-1.97	-31.9	1.87	-5.06	-1.87	6.74	15.17	-16.30	~6.45	<b>15.63*</b>		372.6

## FE Substructure Modeling and Simulation

### Overview of the Modeling Approach

#### *Representative MDOT Substructure Design Case Selection*

After discussions with MDOT Bridge Division, the decision was made to restrict the FE modeling to isolated bents of two representative bridge designs that incorporate current MDOT seismic design practice. The MS 7 Bridge Replacement over the Tallahatchie River has been selected as representative of the multi-column pier case which employs shafts poured below natural ground, and the US51 Bridge over the Long Creek as representative of the trestle case which employs piles driven into natural ground. Details shown on drawings provided by MDOT Bridge Division that affect the modeling of these two bridges are found in Appendix B.

The MS 7 Bridge case is seen to consist of two representative span types. The first type used at the abutments and adjacent approach spans consists of a concrete composite deck system with seven 72 *in* deep, 130 *ft* long, prestressed concrete (PC) bulb-tee (BT 72) girders. The second type used over the river channel and banks consists of a composite deck system with five 3-span continuous 780 (240-300-240) *ft* long, 105 *in* deep steel plate girders. To capture the different tributary mass, bearing gravity load, and corresponding substructure stiffness, separate FE models have been created for each type. Intermediate Bent No. 9 (IB9) has been used to characterize the deck system and substructure for a typical PC girder span, and IB7 to characterize the deck system and substructure for a typical steel girder span.

The US51 Bridge case is seen to consist of one representative span type in interior bents and one at the abutments. The interior bent is the focus here and consists of a concrete composite deck system with seven 63 *in* deep, 135 *ft* long, PC Florida I-Beam (FIB 63) girders. IB5 has been used to characterize the deck system and substructure for a typical span.

#### *Software Selection*

An FE-based structural design and analysis software [10] has been selected for the parametric response analysis of the substructures under lateral loads associated with the deck self-weight and inertia. The computational tool has robust features that include frame (rod, truss, beam) and area (plate) elements for 3D steel and reinforced concrete structural systems. The tool also offers special purpose spring and link elements for enabling interactions to be represented between frame and area elements with one another and with the supports. Special hinges are available for representing inelastic section response. Concentrated masses may be applied at nodal points for developing inertial forces. Figure 3 shows one of the models created for the study. An extruded view is shown highlights fictitious section shapes used for rigid elements between the bearing links and the cap beam frame element. The horizontal soil spring elements

are not visible but are distributed every 5 ft below natural ground.

A more general-purpose solid modeling software [11] has been used to demonstrate some of the potential challenges and benefits of more refined and computationally intensive analysis using the IB7 case under lateral loading at the cap beam level as an example. Figure 3 shows a comparable substructure model created for the study which shows only geometry (topology) defined in the Part module. Reference Points used to define the direction of soil springs (Interactions) are shown by X-marks. The solid element Mesh and Part Interaction features are defined in the Assembly module.

#### *Primary Substructure Systems*

Isolated bents have been modeled to enable parametric evaluation of the bearing lateral load transfer mechanism from deck to substructure during an earthquake. The substructure components have been idealized as six degree-of-freedom (6 DOF) 3D frame elements having prismatic sections. Cap beam sections are concrete rectangles with longitudinal and transverse steel reinforcement. Shafts are circles with longitudinal and spiral steel reinforcement. Details of the sections are provided in Appendix B.

Out of plane movement has been restrained at all nodes defining frame elements to prevent out-of-plane shears and moments from developing. Vertical and lateral movements are therefore resisted only through soil interaction elements described below so that axial force and in-plane shear and moment develop as the frame nodes displace vertically and laterally as dictated by the response to the applied loading.

#### *Superstructure, Bearing, and Soil-Structural Interaction*

The complexity of the deck cross-section geometry requires that self-weight and inertia loads be distributed to the bearing locations in a reasonable manner. Frame and area elements have been used to capture the effective lateral stiffness of the deck system diaphragm and cross-frame at the bents and to maintain the proper location of the centers of gravity and mass of the tributary portions of the deck slab and girders. Tributary slab and girder weights and masses are estimated outside the software using data found in the drawings are applied at these points using the software.

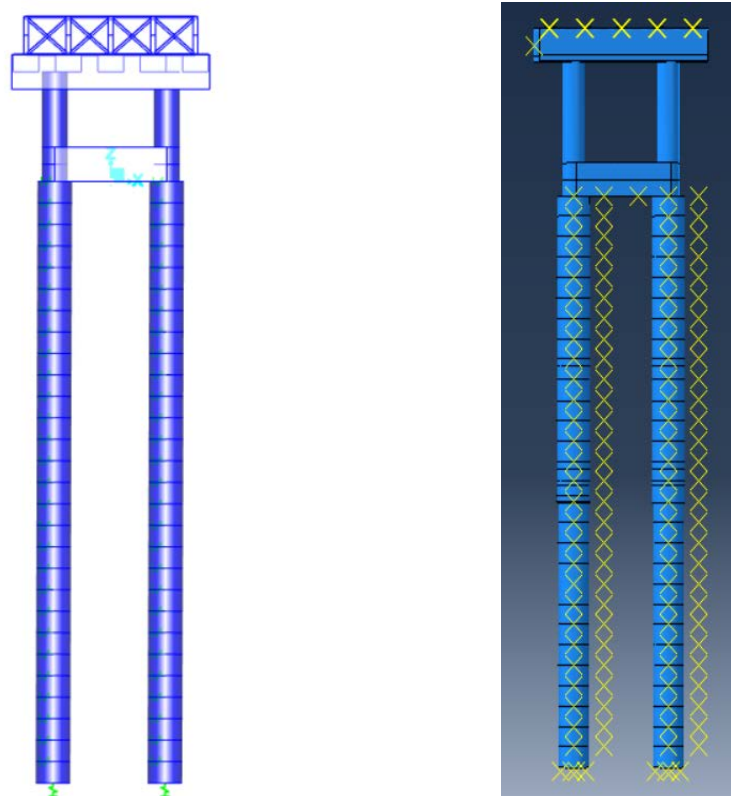


**Figure 3.** Substructure model developed using FE-based structural software [10] (left) and general-purpose software [11] (right)

The complex vertical and lateral load-deformation behavior has been modeled using the Link feature of the software. Calibration/verification analyses were performed on single Link models, and the High Damping Rubber Isolator (HDRI)-type Line Spring was found to be effective for the purposes of this study. Details of this feature are provided in screen captures appearing in Appendix C. The vertical (compression) stiffness was developed by appropriately specifying the axial rigidity of a frame element created between nodes at the top and bottom of the bearing. The lateral (shear) stiffness is entered directly as a Line Spring property in the direction perpendicular to the bearing axis (i.e. parallel to the frame element axis). Figure 4 shows the graphical estimate of the respective stiffnesses using the test data from the comparative experimental study [9] discussed previously.

Soil response to movement of the substructure elements below natural ground has been captured using Simple Joint Springs that may potentially develop a force (or moment) proportional to the displacement (or rotation) of the joint in each of its six DOFs based on the stiffness coefficient input by the user.

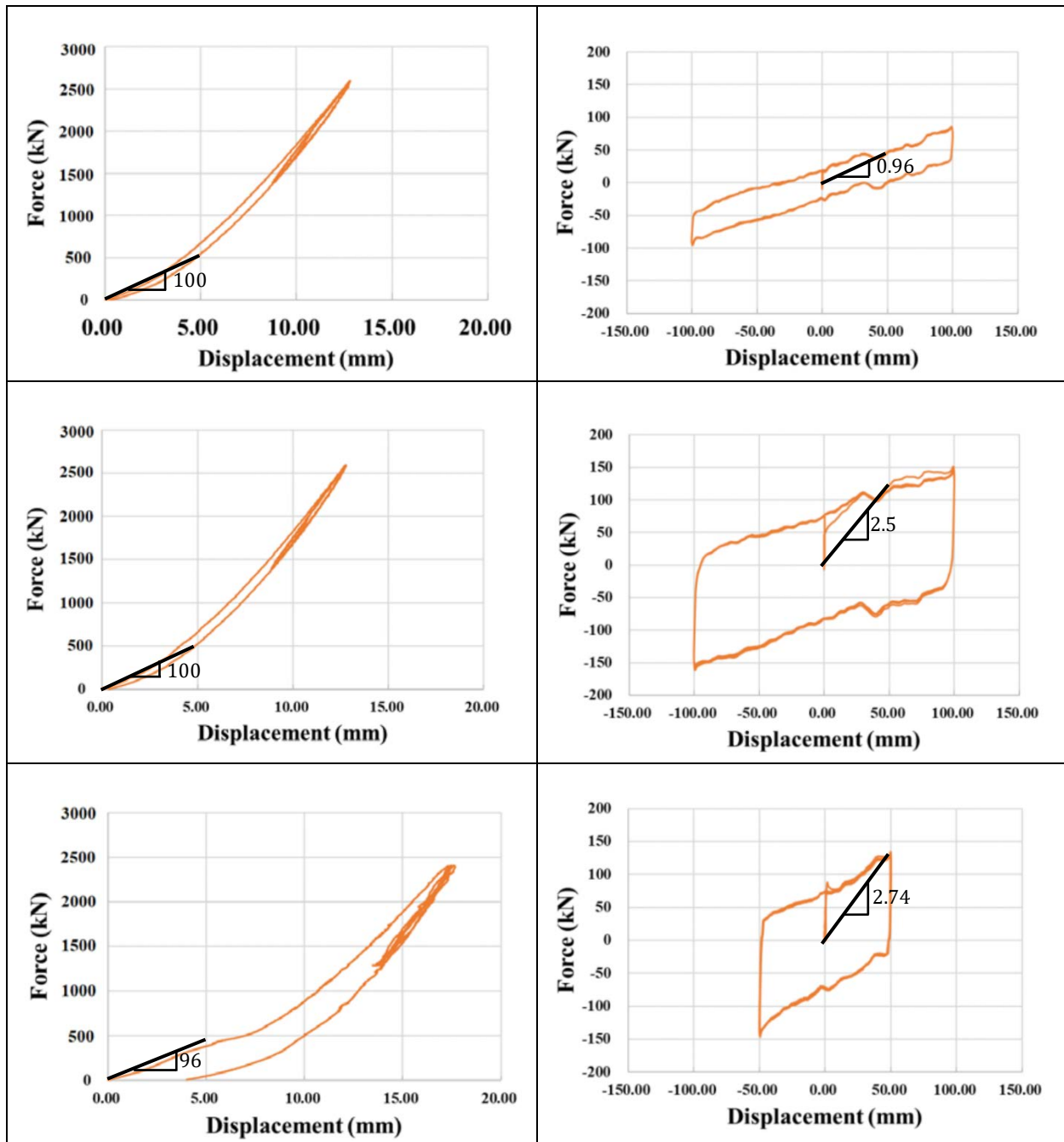


**Figure 4.** Graphical estimate of  $K_{eff}$  used to define Line Spring properties for NRB (top), LRB (mid), and EQS (bot) cases using data from comparative experimental study [9]

Soils information indicated on the MDOT Drawings have been used to establish layer depths and classification. Stiffness coefficients corresponding to these classifications have been selected based on the procedure adopted in a prior study performed by the first author for bridges located in north MS [5]. Figure 5 and Table 2 summarize the results of the layer identification and stiffness calculations, respectively, for the two bridge sites being used as the basis for this study.

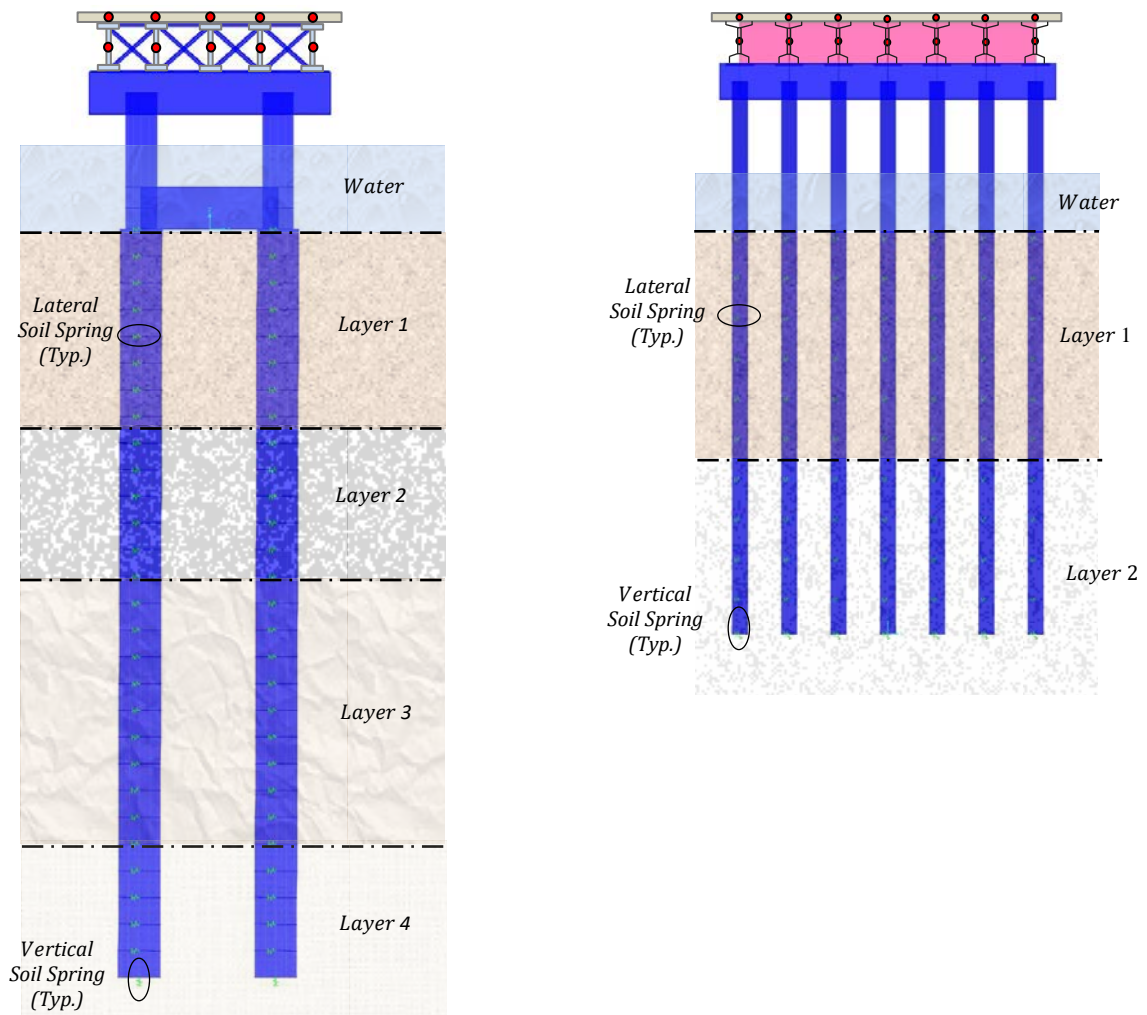


**Figure 5.** Idealized soil profiles for the two-column pier (left) and trestle (right) bridge locations used in the FE modeling.

**Table 2.** Soil spring stiffness estimates using the equivalent circular footing on a half space approach applied in a prior UM study of seismic vulnerability of north MS bridges [5].

Layer	Soil Type	Es (ksi)	B (ft)	H (ft)	Nu	G (ksi)	R (in)	ko (k/ft)
<b>Pier</b>								
1	Soft Clay	2.50	8.0	35	0.50	0.86	280	3221
2	Medium Clay	4.50	8.0	30	0.45	1.55	240	5799
3	Medium Dense Sand	3.25	8.0	55	0.40	1.16	440	3976
4	Sand and Gravel	17.50	8.0	20	0.35	6.48	160	20495
<b>Trestle</b>								
1	Dense Sand and Gravel	9.50	2.5	25		3.28	63	6843
2	Hard Clayey Silt and Sand	5.50	2.5	20		1.90	50	3962

*Deck Load/Mass, Bent System Stiffness, Section Capacity, and Input Time History*

Tributary weights of the girders and deck have been estimated using information shown on the MDOT Drawings in Appendix B. A summary of estimates calculated for the three substructure cases considered in this study is provided in Table 3.

**Table 3.** Bearing dead load estimates.

<b>Case</b>	<b>Girder (k)</b>	<b>Deck (k)</b>	<b>Total (k)</b>
<b>MS7 IB7</b>	166	305	471
<b>MS7 IB9</b>	104	98	202
<b>US51 IB5</b>	145	113	258

Internal force levels will be evaluated relative to section inelastic section capacities using ratios that express a) a direct measure of safety, b) an indirect measure of relative cost, and c) an expectation for inelastic response during strong motion phases of the earthquake simulation. For the columns, shafts, and piles, an estimate of the axial compression (P)-bending moment (M) interaction relationship is needed which accounts for the nonlinear stress-strain behavior of the component concrete and steel materials and the beam-column kinematic assumptions for strain distribution on the section. Both features are incorporated in the software procedure used in this study through the Nonlinear Hinge feature. The feature has been activated in a static deformation-controlled pushover analysis of an isolated cantilever element subject to constant axial load and monotonically increasing lateral load. Such cantilever analyses have been performed to estimate the capacities of the critical reinforced concrete column, shaft, and cap beam, and steel pile sections. Details of this procedure are indicated in screen captures provided in Appendix C.

The input acceleration scenario earthquake time history is taken from a realization of a catastrophic New Madrid Fault Zone (NMFZ) event generated using software provided on request by the US Geological Survey for use in a prior UM study of seismic vulnerability of bridges in north MS [5]. Figure 6 provides a plot of the final record used in this study which has been scaled upward from that of the earlier study to achieve a peak ground acceleration, PGA= 0.36 g, compatible with contour maps generated for north MS in a more recent MAEC study of infrastructure vulnerability in the NMFZ [8].



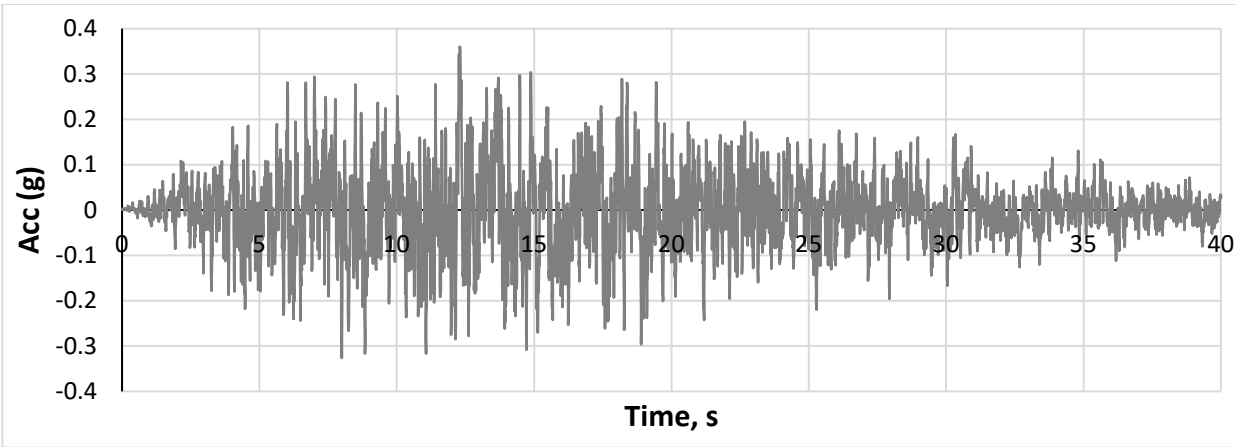


**Figure 6.** Input time history acceleration used for the study based on prior studies [5], [6], [8]

## FE Analysis Results

### *Substructure Lateral Stiffness, System Vibration Frequencies, Section Flexural Capacity*

To aid in understanding the dynamic characteristics of the bent systems, a fourth bearing case has been developed in which the Line Springs have been replaced by a rigid connection. This case thus captures the direct interaction of the superstructure mass and the substructure mass and stiffness without the influence of the bearing stiffness.

Lateral stiffness for the rigid bearing (RGD) case has been estimated for each bent studied using linear static response analysis under a horizontal unit load distributed uniformly over all the bearings in the bent. The total mass of the superstructure is determined by converting the bearing dead load at each girder to mass by dividing by the gravitational constant and multiplying by the number of bearings (girders) in the deck system. The frequency of an effective single DOF (SDOF) system may then be estimated from the elementary vibration theory ( $2 \pi f = \sqrt{k/m}$ ) using the system lateral stiffness at the bearing level for  $k$  and the total mass of the superstructure for  $m$ . Table 4 summarizes the bent lateral stiffnesses and effective SDOF frequencies computed in this manner.

**Table 4.** Estimates of bent lateral stiffness and effective SDOF frequency for RGD bearing case.

Case	Displ (ft)	Stiff (k/ft)	No. Girders	Freq (Hz)
<b>MS7 IB7</b>	1.29E-04	7.75E+03	5	1.64
<b>MS7 IB9</b>	5.33E-04	1.88E+03	7	1.04
<b>US51 IB5</b>	2.05E-04	4.88E+03	7	1.48

Eigenvalue analysis has been performed for each of the bent RGD cases and frequencies and mode shapes determined. Figure 7 shows the deformed shapes of the lateral characteristic mode, and Table 5 summarizes the corresponding natural periods and frequencies.

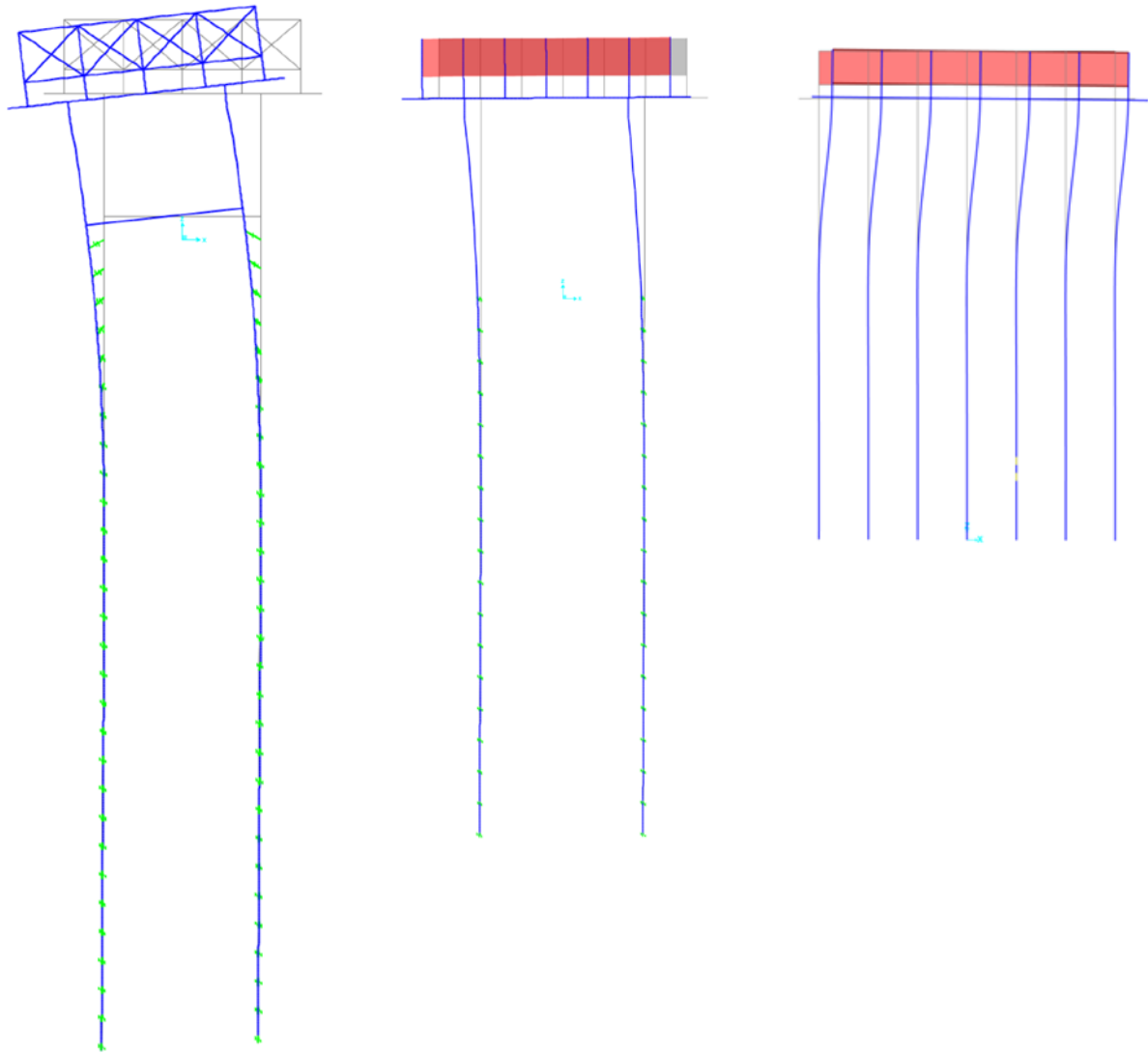


**Figure 7.** Characteristic lateral mode shape computed for RGD cases for MS7 IB7 (left), MS7 IB9 (middle), US51 IB5 (right) (deformation scale and direction are arbitrary)

**Table 5.** Computed natural period and frequency for characteristic lateral mode RGD cases.

Case	Period (s)	Freq (Hz)
<b>MS7 IB7</b>	0.82	1.22
<b>MS7 IB9</b>	1.10	0.91
<b>US51 IB5</b>	0.74	1.35

The SDOF estimate given in Table 4 is found to be similar to the FE model modal analysis result given in Table 5 with a slight overprediction in each case. This is primarily due to the lack of incorporating the distributed substructure mass in the calculation. The deformed shape of the lateral load response is very similar to that of the characteristic lateral vibration mode.

### *Influence of Bearing Effective Stiffness on Vibration Modal Characteristics*

Eigenvalue analysis has been performed for each of the bent non-rigid bearing cases and frequencies and mode shapes determined. Figure 8 shows the deformed shapes of the lateral characteristic mode for each bent type for the NRB case (LRB and EQS are similar), and Table 6 summarizes the first few characteristic frequencies for the three bent types for the three non-rigid bearing cases.

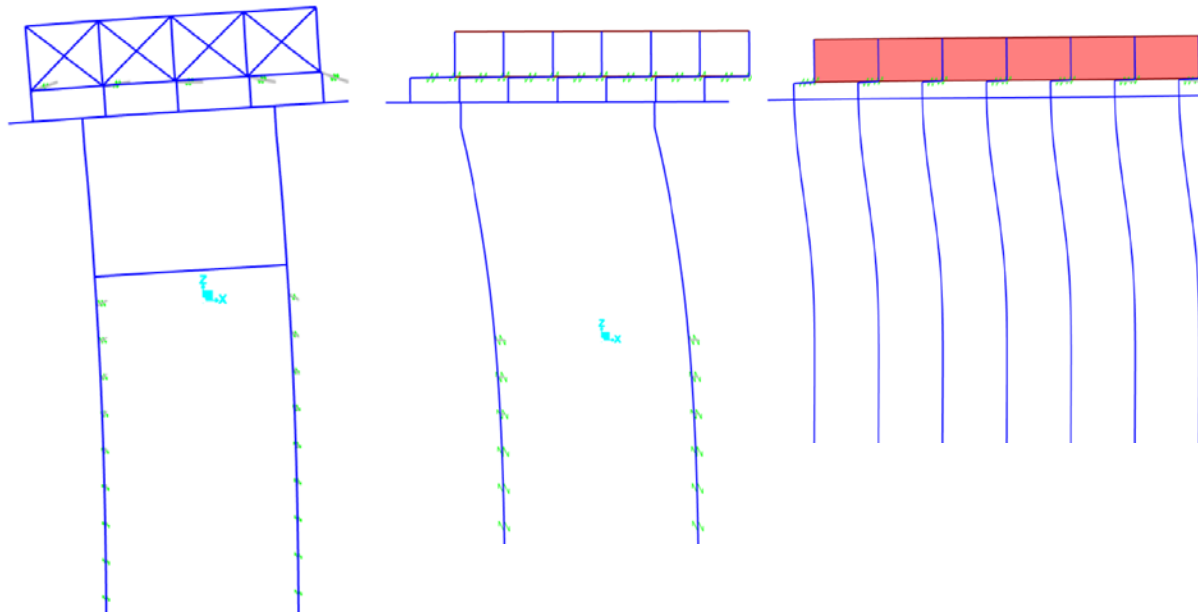


**Figure 8.** Comparison of lateral mode shape computed for the NRB case for MS7 IB7 (left), MS7 IB9 (middle), and US51 IB5 (right) (deformation scale and direction are arbitrary)

Two lateral modes are listed in Table 6. The first lateral mode, when applicable, involves a lateral movement of the superstructure with little or no movement of the substructure which occurs at a lower frequency than the second. The second lateral mode involves lateral movement by both. In Figure 8 the bearing (line) spring orientations indicate that the superstructure and substructure centers of mass move in the same direction for the MS7 IB7 case, whereas they move counter to one another in the other two cases. Comparing bent types, it is apparent that the second lateral mode frequency increases substantially as one goes from the MS7 Bent 7 to the MS7 IB9 two-column pier case and again as one goes from the MS7 IB9 two-column pier case to the US51 IB5 trestle case.

**Table 6.** Computed frequencies for characteristic modes for all bent and bearing cases.

<b>Mode</b>	<b>Lateral 1</b>	<b>Lateral 2</b>	<b>Vertical</b>	<b>Rotation</b>
<b>Bearing</b>	<b>Freq. (Hz)</b>	<b>Freq. (Hz)</b>	<b>Freq. (Hz)</b>	<b>Freq. (Hz)</b>
<b>MS7 IB7</b>				
<b>RGD</b>	NA	1.22	3.68	7.14
<b>NRB</b>	NA	1.26	3.68	7.13
<b>LRB</b>	NA	1.34	3.68	7.14
<b>EQS</b>	NA	1.36	3.68	7.13
<b>MS7 IB9</b>				
<b>RGD</b>	NA	0.91	5.49	5.18
<b>NRB</b>	0.51	2.29	5.49	5.40
<b>LRB</b>	0.82	2.63	5.49	5.41
<b>EQS</b>	0.86	2.68	5.49	5.41
<b>US51 IB5</b>				
<b>RGD</b>	NA	1.35	15.21	15.13
<b>NRB</b>	0.45	4.96	15.19	15.45
<b>LRB</b>	0.72	5.30	15.19	15.45
<b>EQS</b>	0.75	5.34	15.09	15.32

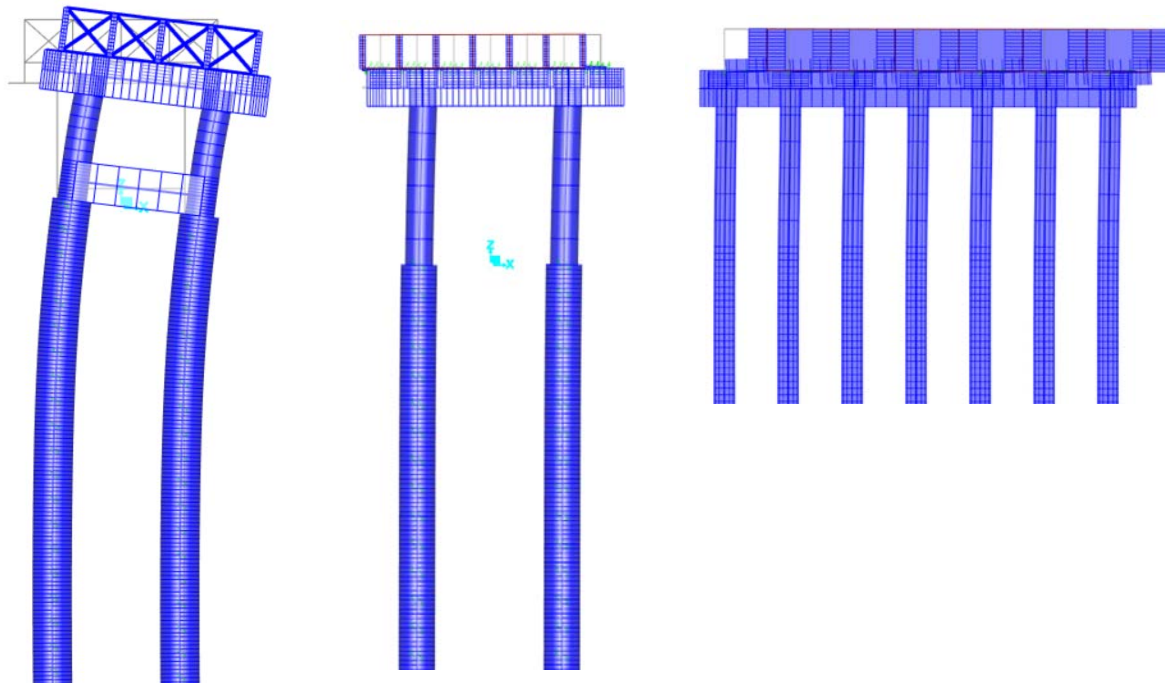
### *Influence of Bearing Effective Stiffness on Earthquake Response*

Linear time history (transient) analysis has been performed for each bent and bearing case using the simulated NMFZ acceleration time history applied to all joints where lateral soil springs are located. Thus, wave propagation (and potentially amplification) upward through the soil-foundation system has been neglected. Default integration (Modal with first 12 modes) and damping (constant  $\xi = 0.05$ ) assumptions have been assumed.

Time varying axial forces ( $P$ ) and in-plane bending moments ( $M3$ ) have been checked in each of the columns and shafts (at positions with soil-springs) to determine the maximum bending response  $M_{max} = \text{Max} \{M3(z, t)\}$  [ $0 < t < t_{max} \approx 40s$ ] and the corresponding axial force. Figure 9 shows sample deformed shapes at time instants found to maximize the bending response in several of the bent and bearing cases. Figure 10 shows bending moment diagrams for these sample cases and time instants. Table 7 summarizes the peak moments in each of the critical substructure elements (column, shaft, pile) for all the cases considered.

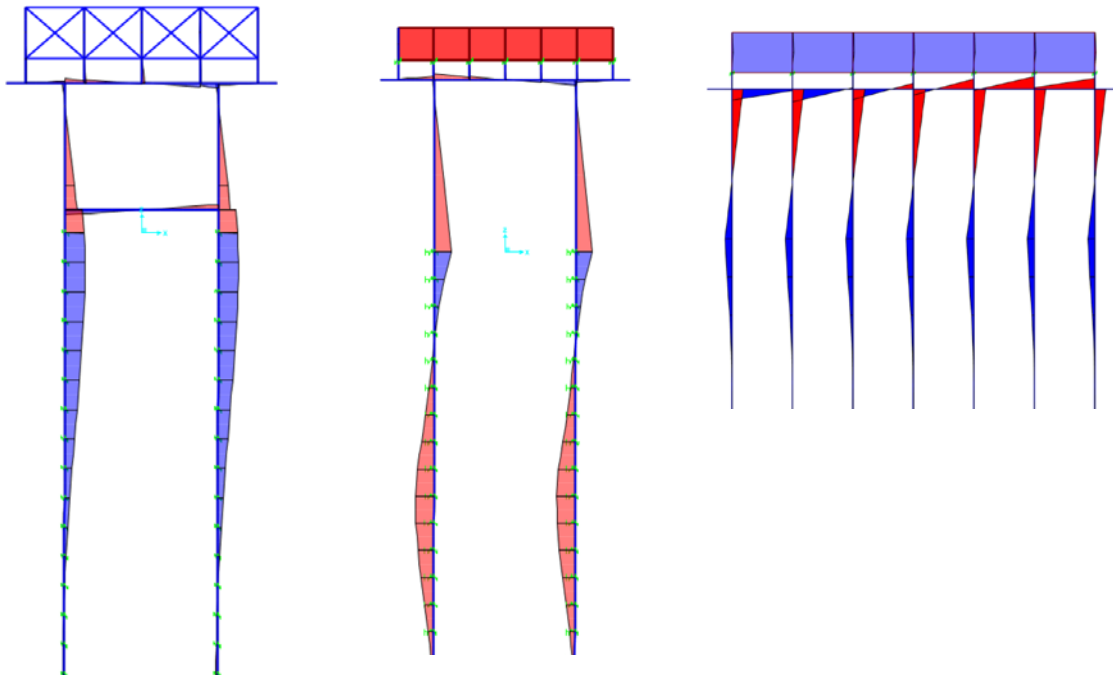
Figure 9 shows the variety of seismic responses of the two-column pier and trestle cases in the presence of a variety of soil-structure interaction and bearing stiffnesses. The RGD case is seen to force the deck to rotate and displace laterally in a cantilever beam type action for the case

with the deeper foundation. Some of the rotation and lateral displacement intensity may be mitigated by relative motion of the deck girders and adjacent piers. The bearings enable more complex dynamic interaction of superstructure and substructure mass. In the case with a seismic bearing and shallower foundation, the two mass centers move counter to one another indicating dominance of the first vibration mode computed for this system. In the case of the trestle with a relatively stiff bearing, however, the two masses move together at the time of peak response although it is difficult to observe this in the plots due to the dominance of the superstructure lateral movement.



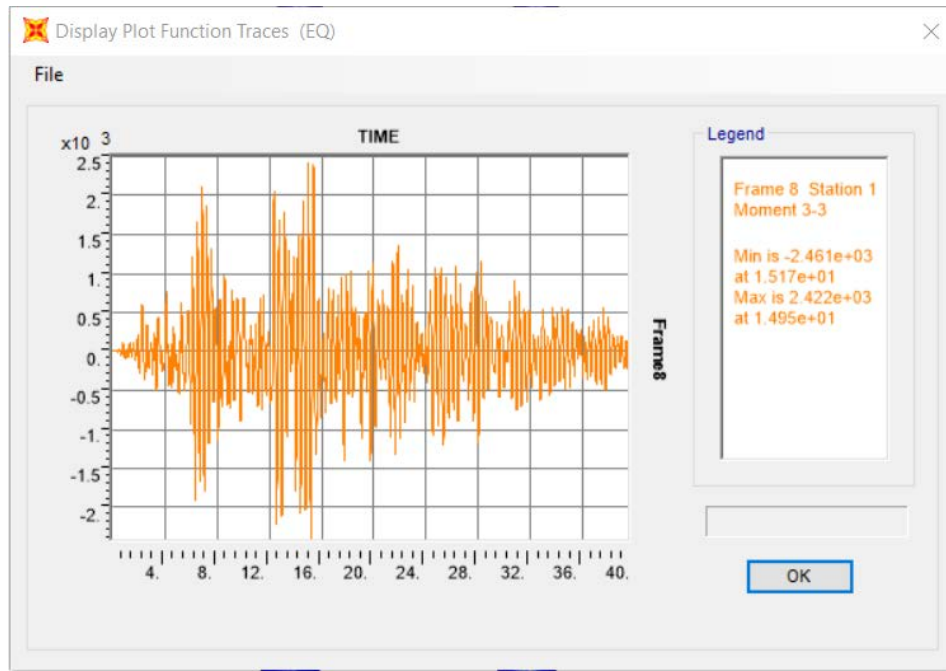
**Figure 9.** Comparison of deformed shapes at time of peak computed bending moment for the MS7 IB7 RGD (left), MS7 IB9 EQS (middle), and US51 IB5 NRB (right) cases

Figure 10 shows the variety of bending action in the substructure elements for the three systems. In the deeper foundation with the strut, the maximum moment in the column occurs at the strut location and the maximum moment in the shaft peaks near the strut and approaches zero at an intermediate depth. In the shallower foundation without a strut but with a seismic bearing, the maximum moment in the shaft occurs near the base and a point of contraflexure develops at intermediate depth. And, in the trestle case, the maximum moment in the pile occurs at the cap beam location with a point of contraflexure at an intermediate depth. In the latter case, the model assumes a rigid connection between pile and cap beam. The real nature of the field connection induces partial rigidity and some of the moment is redistributed to the pile at some depth.



**Figure 10.** Comparison of bending moment diagrams computed for the MS7 IB7 RGD (left), MS7 IB9 EQS (middle), and US51 IB5 NRB (right) cases

Figure 11 shows a typical bending moment time history computed for one of the pier cases with the seismic bearing active. Whereas the input PGA occurs around 12 s (see Fig. 6), the peak bending moment occurs at various times in the strong motion phase (8-20 s) depending on the substructure or bearing case.



**Figure 11.** Typical computed bending moment (M3) time history (MS7 IB9 EQS case, k-ft)

Table 7 summarizes the peak in-plane bending moments calculated using the scenario event simulation for each substructure and bearing type considered. Not shown are time of occurrence and the corresponding axial load in the member at that time although these were recorded as well.

**Table 7.** Comparison of peak bending moments computed for the pier and trestle cases.

	MS7 IB7				MS7 IB9				US51 IB5	
	Column		Shaft		Column		Shaft		Pile	
Bearing	M	M/Mu	M	M/Mu	M	M/Mu	M	M/Mu	M	M/Mu
<b>RGD</b>	7538	0.769	11180	0.521	10710	2.053	11180	0.987	861.7	0.380
<b>NRB</b>	7188	0.733	10320	0.481	3729	0.715	3903	0.345	131.7	0.058
<b>LRB</b>	5963	0.608	9926	0.462	2564	0.491	2703	0.239	124.5	0.055
<b>EQS</b>	5632	0.575	9610	0.447	2461	0.472	2553	0.225	124.3	0.055
<b>Mu</b>	9802		21476		5217		11325		2269	

For purposes of evaluating the relative safety and potential cost benefit of implementing seismic bearings, an effective demand-to-capacity ratio has been computed as the ratio of the peak moment to the capacity  $M_{max}/M_{ult}$  or for short  $M/M_u$ . The capacity  $M_u$  includes the



effect of the interaction with the axial force present at the time the peak moment is reached. For this reason, the pushover analyses described in the previous section were performed for each critical substructure element under the axial load computed at the time the peak moment developed.

#### *Exploratory Solid Modeling of Substructure Response*

The results obtained using the structural frame element modeling are subject to the limitations associated with the frame element theory implemented by the software. To explore these limitations and the relative difficulty of implementing more realistic response through the use of solid element modeling, a model of the MS7 IB7 two-column pier was constructed with an advanced general-purpose tool [11]. While one of the benefits of using the software is the ability to take advantage of the many advanced inelastic and dynamic response features, the decision was made to focus on the model construction and degree to which drawing details could readily be incorporated. With the approval of a longer term project by MDOT Research Division whose scope of work includes full bridge modeling and focuses on long term resilience, the more advanced features will be explored through a more robust approach.

In this study the workflow of model creation began with the transfer of much of the drawing information related to 3D geometry to accurately represent concrete solid regions including cap beam, columns, strut, and shafts as well as steel reinforcement including spiral cages of transverse reinforcement in the columns and extensions of longitudinal steel into the cap beam and shafts.

The top of Figure 12 shows screen captures of the geometry created in the 3D drawing tool [12] for one of the substructures. The geometry was then exported to a format compatible with the Part topology feature in the solid modeling FE software which is shown in the bottom of Figure 12. Each part created was assigned appropriate material and element data for the FE analysis. Boundary conditions (restraints against out of plane movement and soil springs), interactions (Tie Constraints connecting Parts and embedment of steel reinforcement in concrete Parts), and loads applied to the concrete surfaces were then created in the Assembly module. A relatively fine mesh was then generated consistent with the Part and Assembly assignments, and finally analysis was performed according to definitions in the Step Module.

Two loading steps were executed under linear elastic and static assumptions to test the performance of the model. Stresses in the columns were checked under vertical load, and expectations from elementary mechanics of materials theory were confirmed. Figure 13 shows stresses arising in concrete and embedded steel reinforcement elements from application of a unit lateral load that confirm the expectation regarding the location of peak bending stresses in the columns near the strut as well as peak bending stresses in the shafts at some depth.

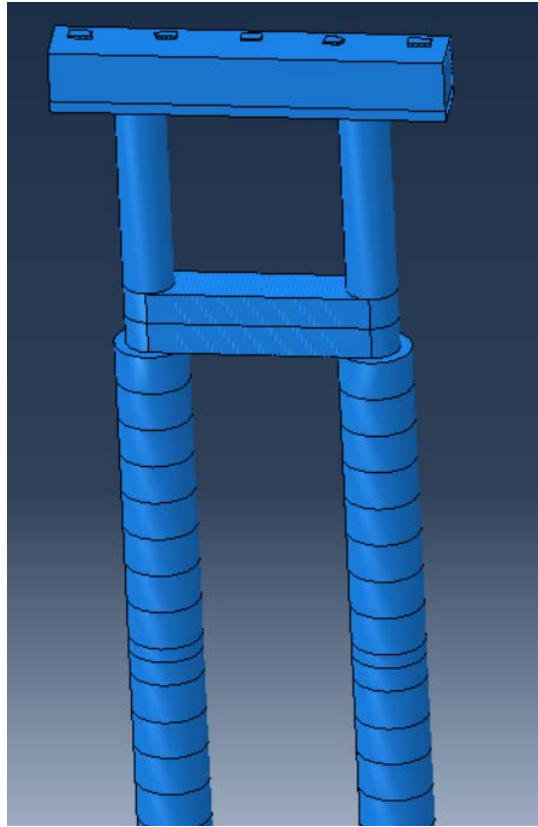
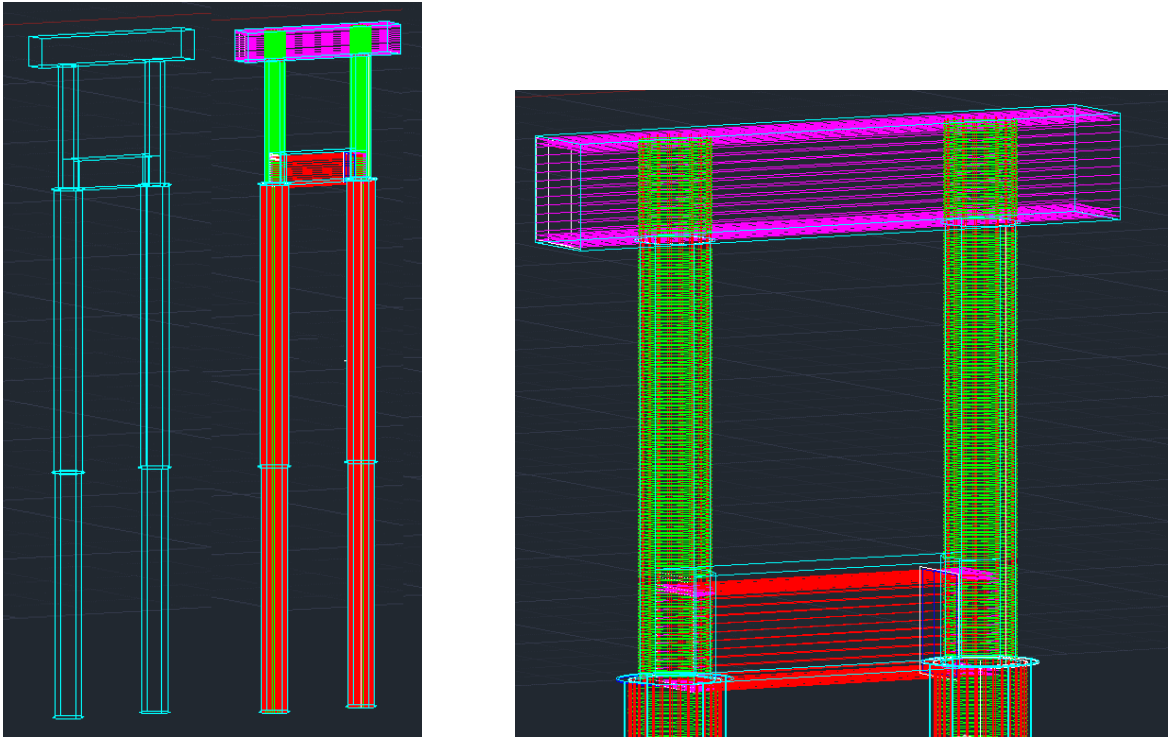


**Figure 12.** Geometry for substructure as created in 3D drawing tool (top left and right) and as imported into solid modeling FE tool (bottom)

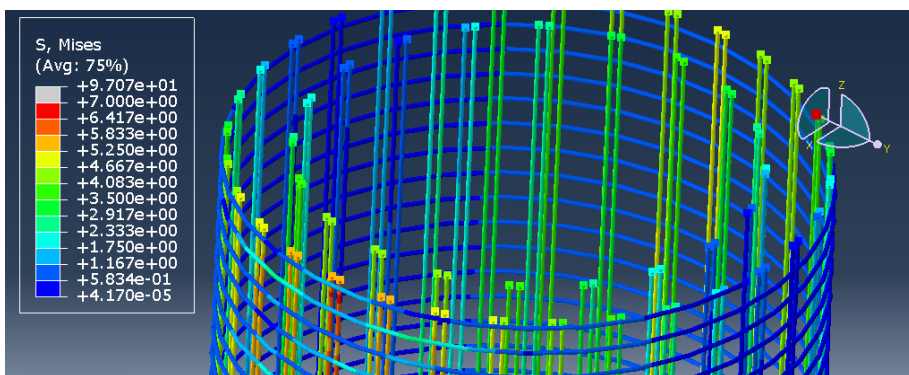
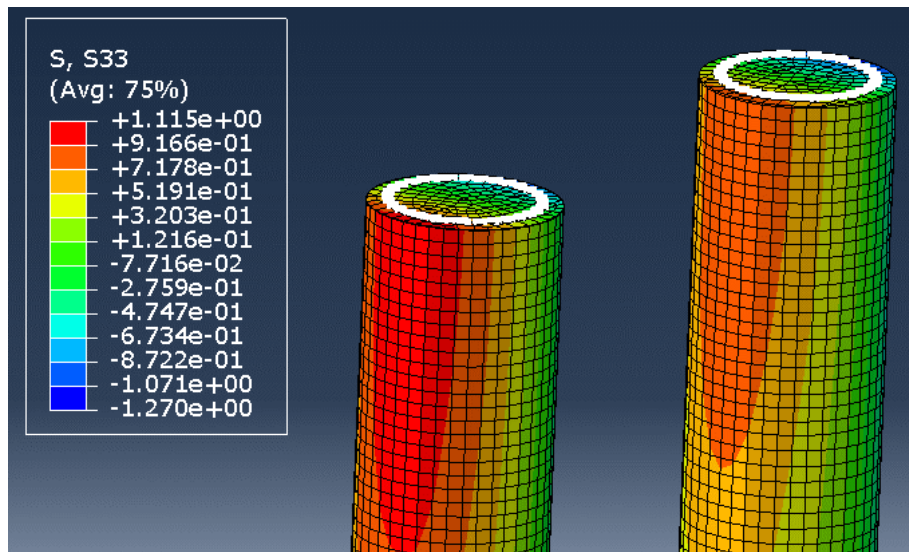
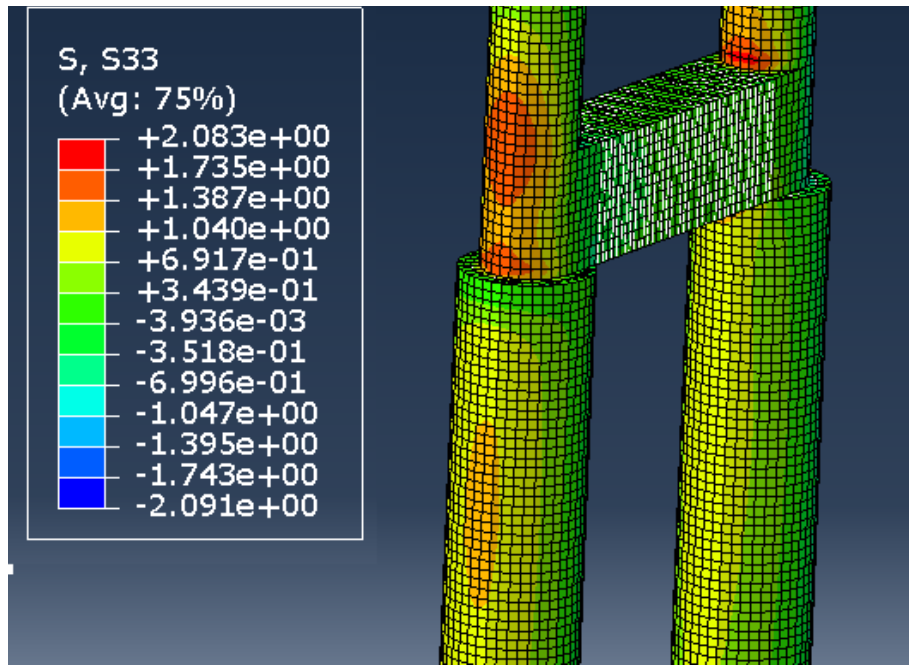


**Figure 13.** Bending stress distribution in concrete substructure elements (top and middle) and in embedded steel reinforcement (bottom) calculated by FE tool for unit lateral load case

## Conclusions

### *Summary*

A literature review has been conducted of off-the-shelf products by suppliers in the United States (US), and a compendium of candidate seismic bearing systems has been developed for potential use by Bridge Division staff that includes 20 companies that manufacture seismic bearing, 22 journal articles discussing research on seismic bearing performance, and 22 universities that have conducted research on seismic bearing performance.

Published load-deformation response behavior of select seismic bearing systems under compression and shear has been examined and experimental data has been identified for use in stiffness parameter estimation to guide structural system modeling and simulation. Estimates of bearing loads have been made for PC spans of MDOT selected two-lane bridges located in north MS and found to consistent with the range of compression loading applied in the testing, and shear deformation in the testing includes the significant range of motion needing to be accommodated in the event of an earthquake. The three bearing systems used in the testing are selected for further study in the FE substructure modeling and simulation.

FE-based models have been created using structural frame and solid modeling software for select cases representing multi-column pier and trestle substructure designs typical of MDOT practice for seismically resistant bridges located in north MS. MDOT drawings for a two-column pier substructure design currently in service and a proposed design for a trestle substructure have been used to define the model geometry, bearing loads, and soil-foundation interactions. The load-deformation measurements in the published comparative experimental study of bridge seismic bearing performance have been used to estimate effective linear bearing stiffness parameters for use in the software. The effective stiffness of soil-foundation interaction elements has been estimated based on a procedure used in a prior MEMA sponsored study of seismic vulnerability of MDOT designed bridges located in north MS.

Static, modal, and earthquake time history analysis has been performed for the select substructure models providing comparative performance of the select seismic bearing types to be evaluated for each substructure model. The time history used in the study corresponds to one generated in a prior UM study sponsored by MDOT with intensity modified to be consistent with a more recent FEMA sponsored study of potential damage and loss to bridges from a catastrophic event in the NMFZ.

### *General Observations from FE Modeling*

The modal analyses indicate that each select substructure type offers unique natural vibration tendencies that are affected in different ways by the seismic bearing stiffness. The seismic

response is affected by these tendencies in complex ways that impact the maximum bending response in the critical substructure members. The study focus has been placed on the substructure columns, shafts, and piles which represent the most significant elements with respect to both safety and cost of construction. Performance of the substructure response with varying bearing stiffness has been characterized through a flexural demand-capacity ratio in the critical members.

#### *Bearing Performance for Two-Column Pier Substructures*

The performance of the two-column pier has been examined with two substructure systems having different superstructure mass due to the different girder types employed (PC and steel plate) and tributary span lengths (130 and 240/360 ft). The heavier, longer-span superstructures are naturally supported by deeper shaft foundations.

The earthquake simulations for the two substructure cases predict a flexural demand-capacity ratio for the columns of between roughly 0.5 and 0.75 for all three bearing cases (NRB, LRB, EQS) considered. The lateral seismic load does not appear to be influential for the shafts with ratios falling roughly between 0.25 and 0.5.

The three bearing cases are distinguished primarily by their effective stiffness. Two of the cases (LRB and EQS) are almost three times stiffer than the third (NRB). The earthquake simulations indicate a significant benefit may be obtained through reduction in the peak bending moment. The computed flexural demand-capacity ratios in the columns supporting the heavier loads are seen to be reduced by 17 and 22 % relative to the more flexible one (NRB). Ratios in the columns supporting the lighter loads are reduced by 31 and 34 %. Ratios in the shafts for both substructure cases are less significant, ranging only from 4-7 %.

#### *Bearing Performance for Trestle Substructure*

The performance of a trestle with vertical steel pipe piles has also been examined. The superstructure in this case consists of a slightly wider deck slab, shallower PC girders, and a tributary span length of 135 ft.

The earthquake simulations for the two substructure cases predict a very low flexural demand-capacity ratio for the piles of roughly 0.06 for all three bearing cases (NRB, LRB, EQS) considered. Consequently, the ratio reductions for the stiffer bearings, which are found to be only roughly 6% relative to the more flexible one, are of little importance for this substructure case.

As a final observation, the findings of the FE modeling and simulation must be viewed in the context of the limited scope of the study. Many factors possibly affecting performance have

been neglected including 1) longitudinal horizontal seismic motion causing out-of- plane bending of the substructures, 2) relative lateral movement of adjacent substructures causing deformation of the superstructure, and 3) loads unrelated to seismic motions such as vehicular, wind, and flood. Further, many simplifying assumptions have been made in the modeling and simulation including 1) linear elastic material behavior, 2) use of the effective stiffness for the bearings, 3) use of a single synthetic time history, 4) linear soil springs, and 5) use of simplified method for determining soil spring constants.

## Implementation Plan/Recommendations

The results of the present study of seismic bearing performance demonstrates and quantifies potential reductions that may be achieved for the in-plane flexural demand in critical elements of MDOT bridge substructures exposed to the earthquake hazard in north MS. Two of the seismic bearings show promise in achieving significant enough reductions that substantial cost savings may be possible through their use.

The literature review provides a resource for further investigation by MDOT Bridge Division staff of seismic bearing performance and impacts. It was generally observed through the review however that there is a lack of publicly available data on load-deformation characteristics of some of the bearing systems needed for comparative evaluations. To enable further in-depth study of bearing performance for the bridges of interest to MDOT will require more and possibly long-term engagement with some of the primary vendors and potentially some of the research institutions that perform testing.

The FE modeling and simulation demonstrated the complexity of the dynamic and nonlinear behaviors needing to be better understood and quantified to accurately predict the influence of bearing load-deformation characteristics on internal forces in the bridge structural system. Structural frame analysis was found to be useful to obtain initial insights over a range of parameters and assumptions using computational capability typical of a design office.

Solid modeling enables more complex behavior to be examined in regions of critical response. The limited attempt at such modeling in this study revealed that major mesh generation challenges are encountered in interface regions. For the two-column pier substructure studied, the regions requiring particular care were those surrounding elements critical to the proper transmission of load from the girders to the shafts. Some meshing issues were associated with the embedment of steel reinforcement in the cap beam where spiral circular column reinforcement intersects the longitudinal and transverse reinforcement of the rectangular cap beam. Further, the embedment of the intersecting reinforcement occurs very close to the bearing contact surface at the top of the cap beam.

To achieve a mesh resolution using the algorithms of the software required selection of a mix of element types (hexahedral and tetrahedral) as well as a fine mesh. The final mesh resulted in a very large number of DOF and associated computational capacity in order to obtain a system response even for a single substructure subsystem (pier) under static loading assuming linear elastic material behavior. High-performance computing (HPC) will likely become a necessity should this modeling approach be used to simulate the far more computationally intensive nonlinear and dynamic response calculations for a full-bridge model subject to earthquake motion.

Given the findings that were obtained and the challenges that were discovered through the study, it is recommended that MDOT Bridge Division consider additional exploration of the benefits of seismic bearing performance through a combination of external research and internal design activities. An opportunity exists in the short term to further explore some of the limitations of the current study through the full-bridge modeling component of the new MDOT sponsored UM study that focuses on improving resilience of bridges through use of integrated technologies. The new study provides the opportunity for closer engagement between UM research faculty and students and MDOT Bridge Division design and modeling staff. Such interaction could enable further exploration of the broader design process that involves evaluation of multiple loadings and execution of LRFD procedures required by US practice and MDOT policy. It could also enable a more detailed estimation of bearing performance impacts on overall benefits in terms of both design and construction costs.



## References

1. AASHTO Guide Specifications for LRFD Seismic Bridge Design, 2<sup>nd</sup> edition, 2011.
2. (2013) "Seismic Design Policy Manual for Highway Bridges," version 1.0, MDOT Bridge Division (24 pp.)
3. Ervin E K. (2022) <https://ekervin14.github.io/webpage/MFDL.html> , Multi-Functional Dynamics Lab, University of Mississippi.
4. Daves M, Ervin E K, and Zeng C. (2020) "Experimental data interpretation using genetic algorithm for global health assessment of reinforced concrete slabs subjected to cracking." *Advances in Structural Engineering*, 24[147]: 411-421
5. Mullen C. (2002) "Seismic Vulnerability of Existing Highway Bridge Substructures Supporting the I-55 Undercrossing at MS302 (Goodman Road), Final Report submitted to MDOT Bridge Division, MDOT Project No. SP-9999-00(27 101411/011000 [79-999-00-027-11 PE] (133 pp.)
6. Mullen C. (2011) "Seismic Vulnerability of Critical Bridges in North MS." Final Report submitted to Mississippi Emergency Management Agency, FEMA Grant/Contract No. PDMC-04-MS-2009 [CFDA No. 97.047], Center for Community Earthquake Preparedness, University of Mississippi (64 pp.)
7. Mullen C, Ervin E K. (2016) "Detecting Weakened Highway and Railroad Bridge Substructures at Deck Level," Final Report submitted to National Center for Intermodal Transportation Economy and Competitiveness, NCITEC Project No. UM 2013-26, Department of Civil Engineering, University of Mississippi (57 pp.)
8. Elnashai A S et al. (2009) "Impact of New Madrid Seismic Zone Earthquakes on the Central USA: Volume 1," MAE Center Report No. 09-03 (153 pp.)
9. Cho C B, Kim Y J, Chin W J, and Lee J-Y (2020). "Comparing Rubber Bearings and Eradi-Quake System for Seismic Isolation of Bridges," *Materials*, 13 [5247]: 1-10
10. SAP2000, version 21. (2021) Computers and Structures, Inc., Berkeley, CA
11. Abaqus/CAE, version 2020. (2020) Dassault Systemes, Johnston, RI
12. AutoCAD, version 2023. (2022) AutoDesk, Inc.

## Appendix A Compendium of Seismic Bearing Literature

### A1. List of Examined Companies

1. RJ Watson
2. Voss
3. CON-SERV Inc.
4. DS Brown Company
5. Bowman Construction Supply
6. Zaoqiang Dacheng Rubber Co, Ltd. / Sino Technology
7. Bridgestone
8. Tensa
9. Scougal Rubber Corporation
10. Cosmec Inc.
11. Chemtura
12. Hanna Rubber Company
13. Denver Rubber Company
14. Vibrasystems, Inc.
15. BRP Manufacturing
16. GRT Rubber Technologies
17. Warco Biltrite
18. JVI, Inc.
19. American Biltrite
20. Williams Products

## A2. List of Journal Papers

1. Chang Beck Cho, Young Jin Kim, Won Jong Chin, and Jin-Young Lee. Comparing Rubber Bearings and Eradi-Quake System for Seismic Isolation of Bridges. *Materials* 2020, 13, 5247: 1-11.
2. M.C. Constantinou, I. Kalpakdis, A. Filiatrault, and R.A. Ecker Lay. LRFD-Based Analysis and Design Procedures for Bridge Bearings and Seismic Isolators. MCEER Earthquake Engineering to Extreme Events, Univ. of Buffalo, NY, Technical Report MCEER-11-0004, September 26, 2011: 1-436.
3. Pengru Deng, Zhiping Gan, Toshiro Hayashikawa, and Takashi Matsumoto. Seismic response of highway viaducts equipped with lead-rubber bearings under low temperature. *Eng. Structures*, 2020, 209: 110008.
4. Sattar Dorafshan, Kristopher R. Johnson, Marc Maguire, Marvin W. Halling, Paul J. Barr, and Michael Culmo. Friction Coefficients for Slide-In Bridge Construction Using PTFE and Steel Sliding Bearings. *J. Bridge Eng.*, 2019, 24(6): 04019045.
5. Samer El-Bahey and Michel Bruneau. Structural Fuse Concept for Bridges. *Transportation Research Record: Journal of the Transportation Research Board*, No. 2202, 2010, 167–172.
6. Dongming Feng and Fangyin Zhang. Seismic Isolation Retrofitting of Typical Multi-Span Steel Girder Bridges in New York State. *Transportation Research Record*, 2020, 2674(8): 785–798.
7. Liwei Han, Konstantinos V. Belivanis, Todd A. Helwig, John L. Tassoulas, Michael D. Engelhardt, and Eric B. Williamson. Field and computational investigation of elastomeric bearings in high demand steel girder application. *J. of Constr. Steel Res.*, 2019, 162: 105758.
8. Afraa Labiba Hassan and AHM Muntasir Billah. Influence of ground motion duration and isolation bearings on the seismic response of base-isolated bridges. *Eng. Structures*, 2020, 222: 111129.
9. Francesco Lo Monte, Chiara Pozzuoli, Elena Mola, and Franco Mola. Seismic Vulnerability Assessment and Retrofitting Design of a Multispan Highway Bridge: Case Study. *J. Bridge Eng.*, 2018, 23(2): 05017016.
10. Gennaro Magliulo, Vittorio Capozzi, Giovanni Fabbrocino, and Gaetano Manfredi. Neoprene–concrete friction relationships for seismic assessment of existing precast buildings. *Eng. Str.*, 2011, 33: 532–538.
11. Shashank Mala, Eyosias Beneberu, and Nur Yazdani. Hydrocarbon Fire Performance of Reinforced Elastomeric Bridge Bearing Pads. *J. Perform. Constr. Facil.*, 2019, 33(4): 04019038.
12. Stergios A. Mitoulis, Ioannis A. Tegos, and Kosmas C. Stylianidis. Cost-effectiveness related to the earthquake resisting system of multi-span bridges. *Eng. Str.*, 2010, 32: 2658-2671.
13. A. Mokha, M.C. Constantinou, and A.M. Reinhorn. Teflon bearings in aseismic base isolation: Experimental studies and mathematical modeling. NCEER, Univ. of Buffalo, NY, Technical Report NCEER-88-0038, December 5, 1988: 1-214.
14. Samim Mustafa and Chitoshi Miki. Design of Rupture Strength of Side Blocks in Elevated Steel Girder Bridges with Elastomeric Bearings. *Int. J. of Steel Str.*, 2020, 20(3): 885–896.

15. Y. Pan, A. K. Agrawal, M. Ghosn, and S. Alampalli. Seismic Fragility of Multispan Simply Supported Steel Highway Bridges in New York State. I: Bridge Modeling, Parametric Analysis, and Retrofit Design. *J. Bridge Eng.*, 2010, 15(5): 448-461.
16. Sun-Kyu Park, Hyeong-Yeol Kim, and Jung-Hyuk Kim. Bearing Replacement for Prestressed Concrete I-Girder Bridges. *J. Bridge Eng.*, 2001, 6(4): 271-275.
17. Fatemeh Shaker and Alireza Rahai. Substructure Responses of a Concrete Bridge with Different Deck-to-Pier Connections. *Int. J. of Civil Eng.*, 2019, 17(11): 1683-1695.
18. Shahrokh Shoeibi, Mohammad Ali Kafi, and Majid Gholhaki. New performance-based seismic design method for structures with structural fuse system. *Eng. Structures*, 2017, 132:745-760.
19. John F. Stanton, Charles Roeder, and T. Ivan Campbell. High-Load Multi-Rotational Bridge Bearings. NCHRP Report 432, Univ of WA, Transportation Research Board, National Research Council, National Academy Press, Washington, DC., 1999: 1-413.
20. John F. Stanton, Charles W. Roeder, Peter Mackenzie-Helnwein, Christopher White, Colin Kuester, and Brianne Craig. Rotation Limits for Elastomeric Bearings. NCHRP Report 596, Univ. of WA, Transportation Research Board, National Academy of Sciences, 2008: 1-65.
21. Niel C. Van Engelen. Rotation in rectangular and circular reinforced elastomeric bearings resulting in lift-off. *Int. J. of Solids and Str.*, 2019, 168: 172–182.
22. Jiang Yi, Junyong Zhou, and Xijun Ye. Seismic evaluation of cable-stayed bridges considering bearing uplift. *Soil Dyn. and Eq. Eng.*, 2020, 133: 106102.

### **A3. List of Universities**

1. Amirkabir University of Technology, Department of Civil and Environmental Engineering, Tehran, Iran.
2. Aristotle University of Thessaloniki, School of Engineering, Department of Civil Eng., Division of Structural Engineering, Thessaloniki, Greece.
3. The City College of the City, Univ. of New York, Dept. of Civil Engineering, New York, NY.
4. Columbia University, New York, NY.
5. Guangzhou University, College of Civil Engineering, Guangdong, China.
6. Hokkaido University, Engineering, Hokkaido, Japan.
7. Korea Institute of Civil Engineering and Building Technology, Korea, Department of Infrastructure Safety Research.
8. Kyungpook National University, Korea, School of Agricultural Civil & Bio-industrial Engineering.
9. Lakehead University, Department of Civil Engineering, Thunder Bay, ON, Canada.
10. Politecnico di Milano, Dept. of Civil and Environmental Engineering, Milan, Italy.
11. Semnan University, Civil Engineering, Semnan, Iran.
12. State University of New York at Buffalo, National Center for Earthquake Engineering Research (NCEER) Laboratory, Buffalo, NY.
13. Sungkyunkwan University, Dept. of Civil Engineering, Jangan-Gu, Suwon, Kyonggi-Do, Korea.
14. Tokyo City University, Advanced Research Laboratories, Tamazutsumi, Setagaya, Tokyo, Japan.
15. University of Molise, Department SAVA, Engineering & Environment Division, Engineering & Environment Division, Campobasso, Italy.
16. University of Naples Federico II, Department of Structural Engineering, Napoli, Italy.
17. University of Technology, Dalian, China, School of Civil Engineering, Dalian.
18. University of Texas at Arlington, Dept. of Civil Engineering, Arlington, TX.
19. University of Texas at Austin, Austin, TX.
20. University of Washington, Seattle, WA.
21. University of Windsor, Department of Civil and Environmental Engineering, Windsor ON, Canada.
22. Utah State University, Dept. of Civil and Environmental Engineering, Logan, UT.

## Appendix B MDOT Design Drawings

### *MS 7 Bridge Replacement over the Tallahatchie River*

The substructure example used in this study to represent MDOT design and construction practice for a seismically resistant multi-column pier is the reinforced concrete two-column shaft supported system. The photographs below were taken by the first author on June 10, 2015, when the bridge had just been completed. They depict critical substructure elements including a) above ground RC frame (columns, cap, and strut), b) composite deck, c) 3-span continuous steel plate girders and cross-frames, d) disc bearings, e) simple span PC bulb-tee girders and RC columns, f) RC diaphragms and rectangular neoprene pads.











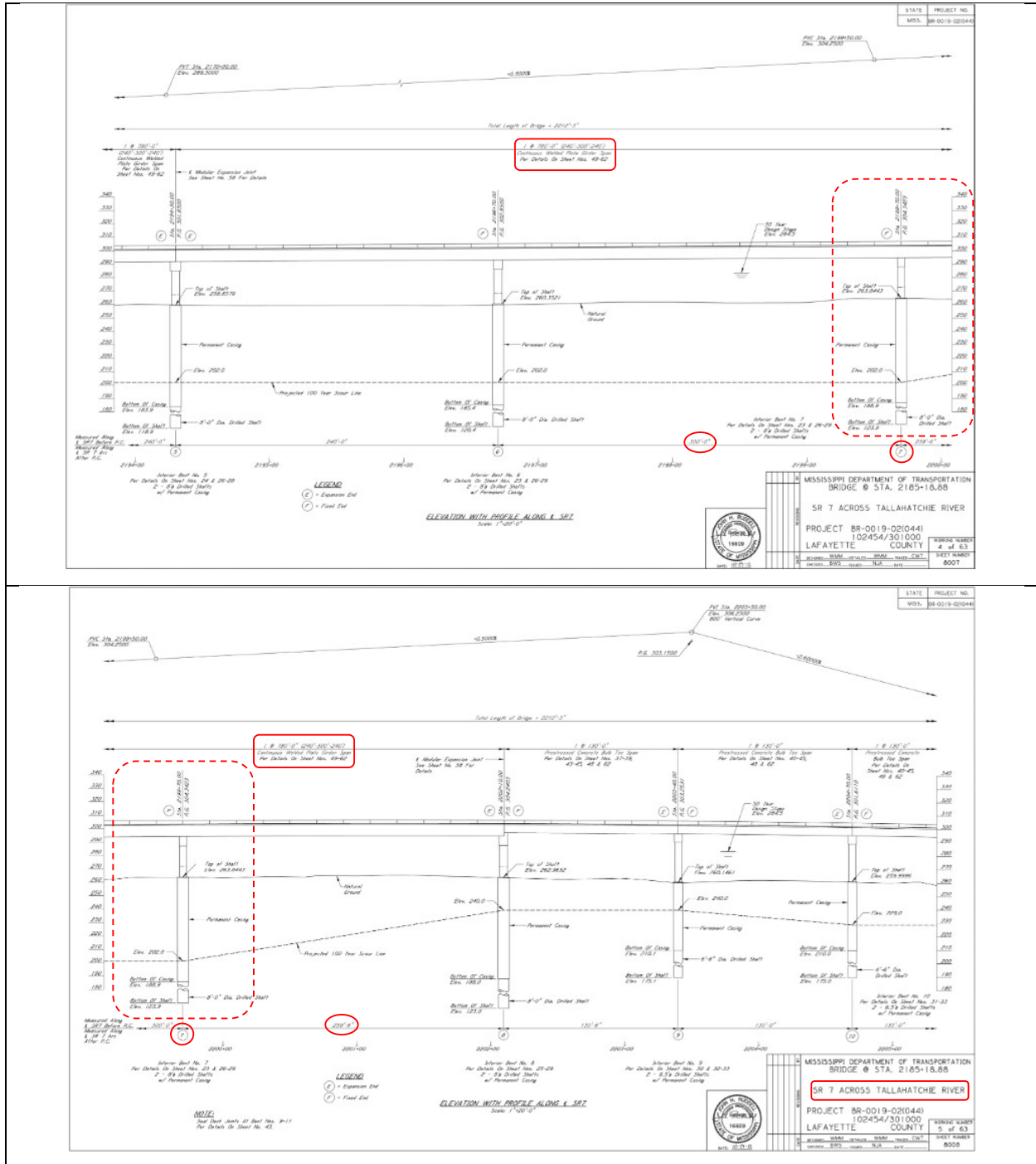


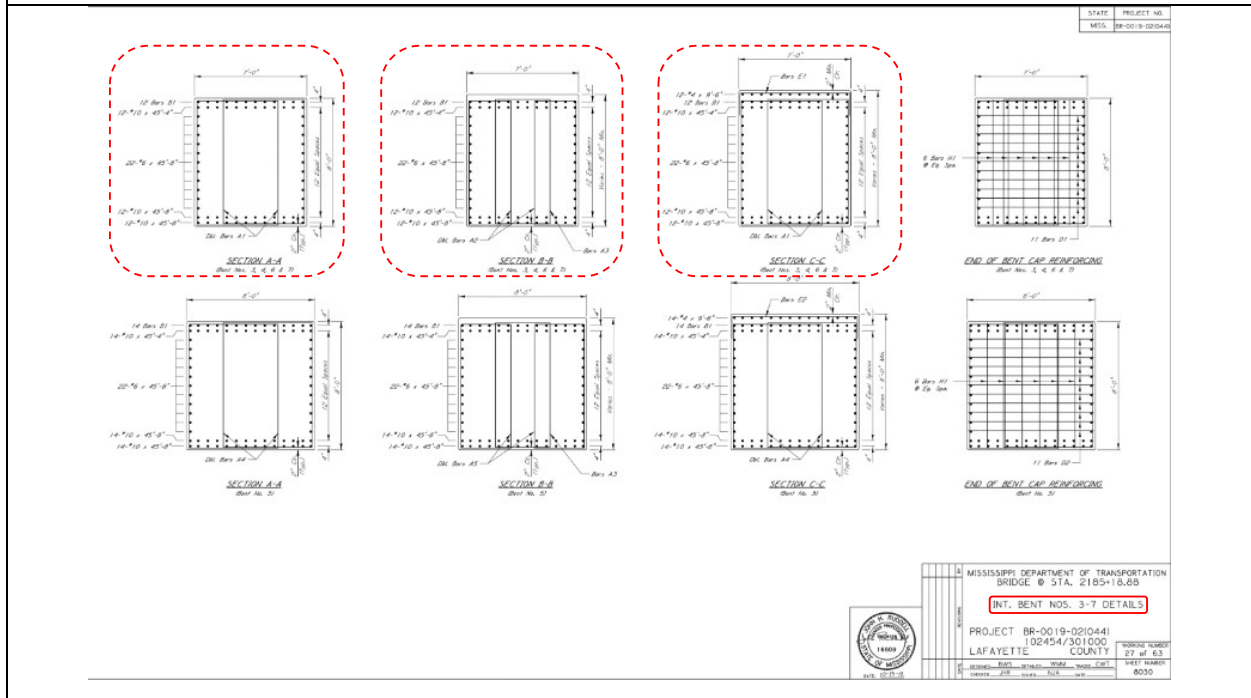
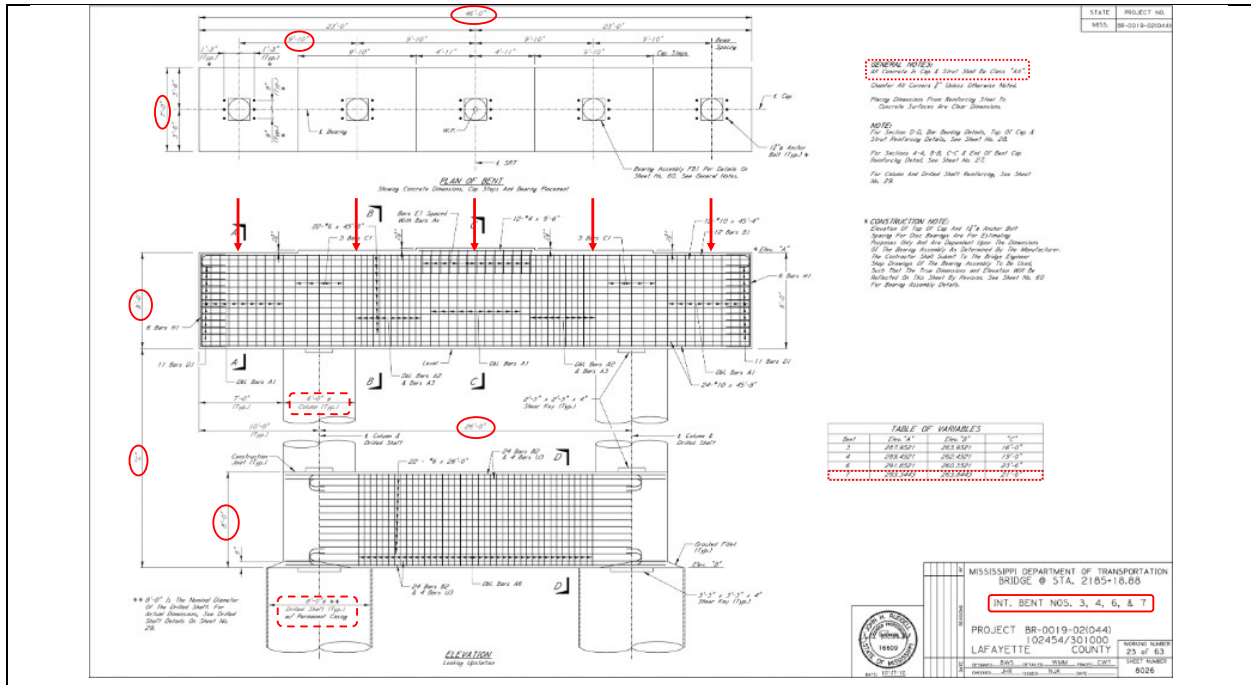




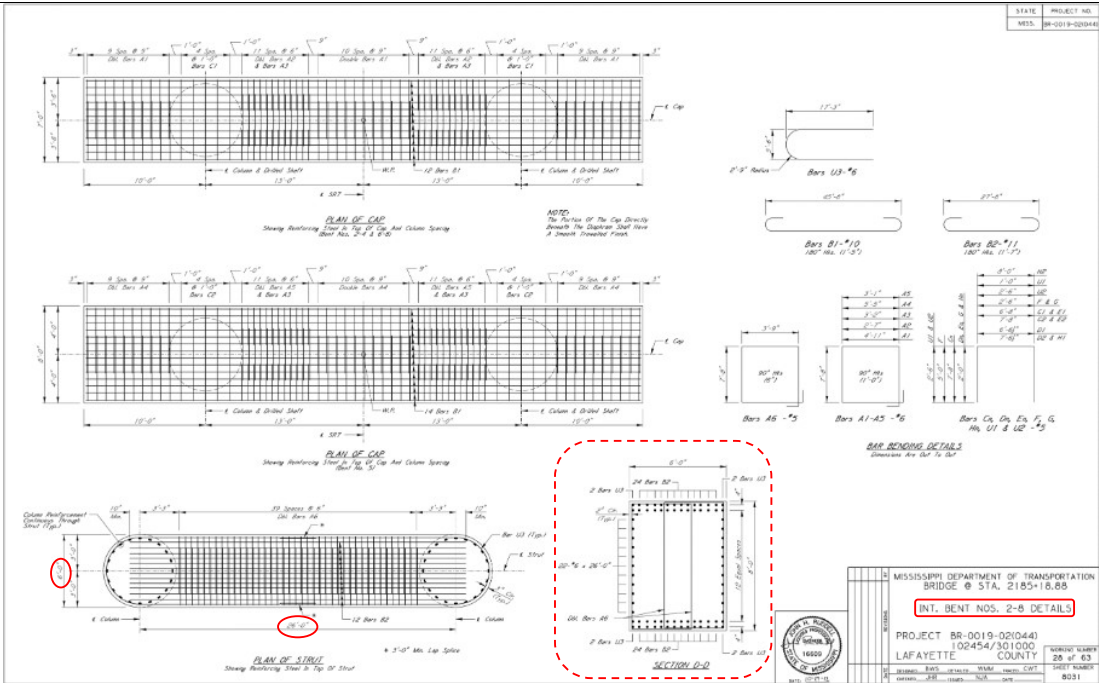
The excerpts below of drawings provided by MDOT Bridge Division depict the details of these critical elements.

**MS7 Substructure for 3-span Continuous Steel Plate Girders (including Bent 7)**





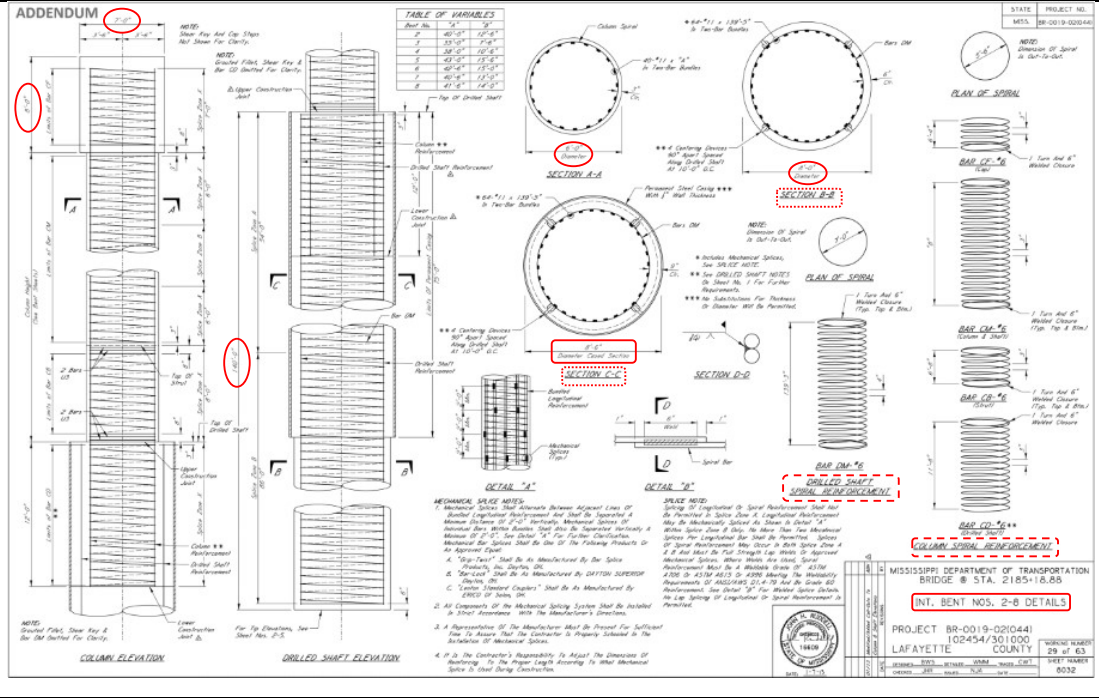




MISSISSIPPI DEPARTMENT OF TRANSPORTATION  
BRIDGE @ STA. 2185+18.85  
INT. BENT NOS. 2-8 DETAILS

PROJECT BR-0019-021044  
102454/301000  
LAFAYETTE COUNTY

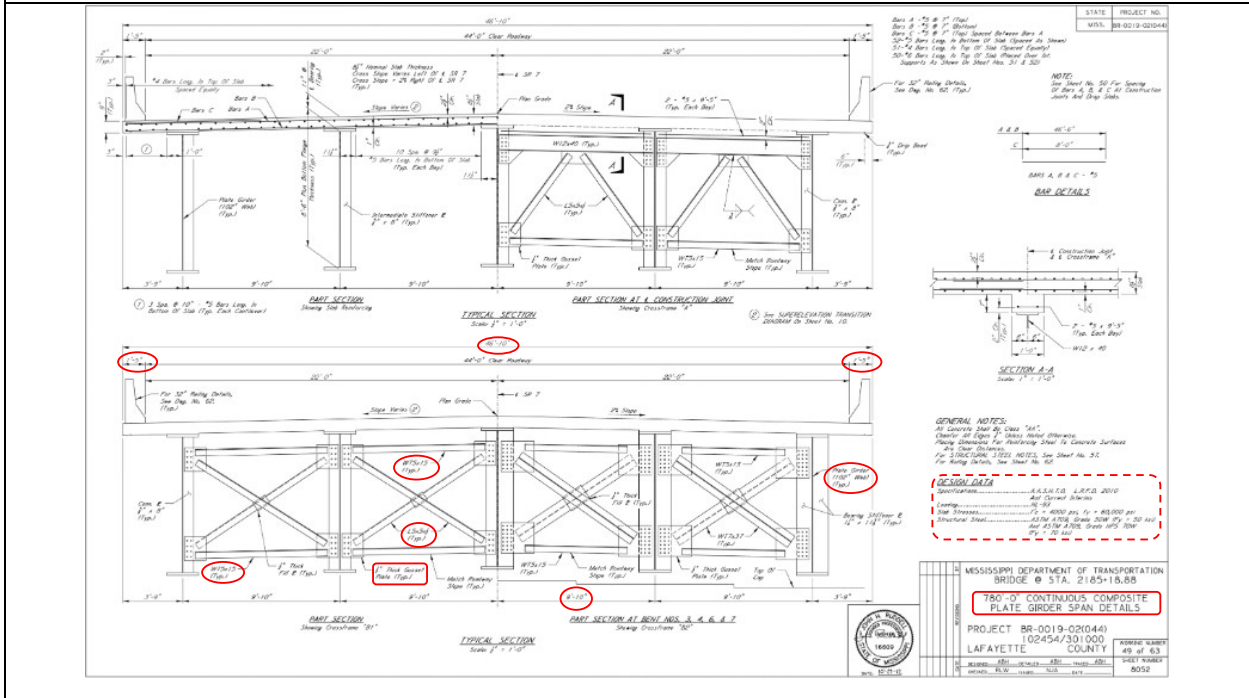
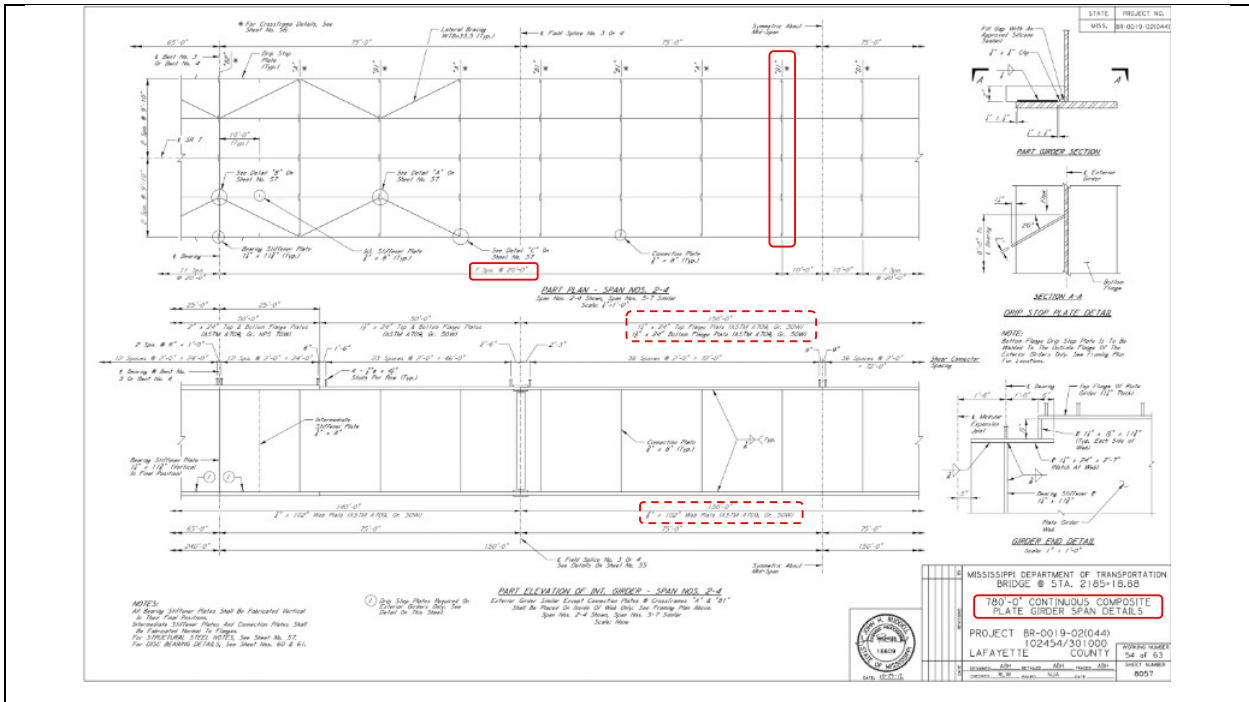
DATE: 11-13-15  
DRAWN: JSS  
CHECKED: JSS  
SCALE: 1/8" = 1'-0"

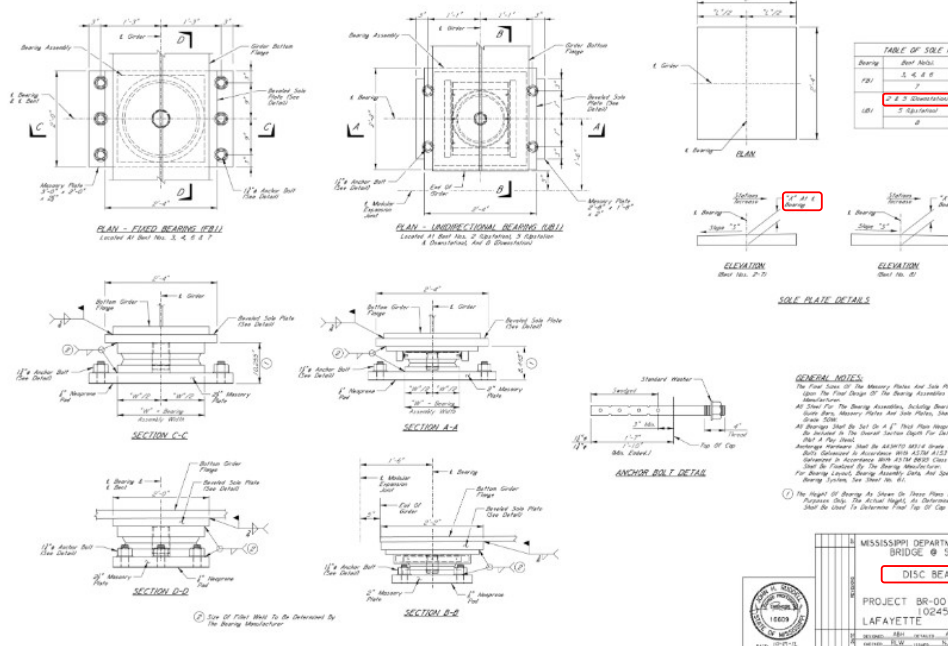


MISSISSIPPI DEPARTMENT OF TRANSPORTATION  
BRIDGE @ STA. 2185+18.85  
INT. BENT NOS. 2-8 DETAILS

PROJECT BR-0019-021044  
102454/301000  
LAFAYETTE COUNTY

DATE: 11-13-15  
DRAWN: JSS  
CHECKED: JSS  
SCALE: 1/8" = 1'-0"





**1st O.REV.**

**SPECIAL NOTES ON STRUCTURAL BEARING SYSTEM**

**DESIGN**  
 The steel shall consist of Forming Multi-Directional High Load Disc Bearings and Infilling Steel. The steel shall be manufactured from Forming Multi-Directional High Load Disc Bearings and Infilling Steel. The steel shall be manufactured from Forming Multi-Directional High Load Disc Bearings and Infilling Steel. The steel shall be manufactured from Forming Multi-Directional High Load Disc Bearings and Infilling Steel.

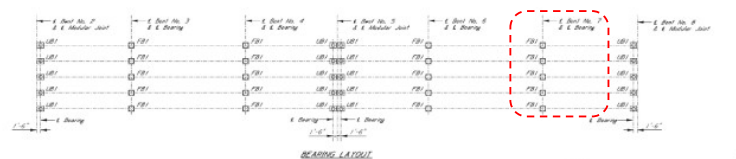
**CONSTRUCTION**  
 All materials shall be as indicated, with no substituted materials incorporated in the finished bearing. The physical properties of the materials shall conform to the requirements of the applicable specifications.

**BEARING ASSEMBLY DATA AND DESIGN REQUIREMENTS**

Quantity	Structural Steel	Forming Steel
Disc	20	20
Sub-Plate	20	20
Anchor Bolt	20	20

**DESIGN REQUIREMENTS**

- The bearing shall be designed to carry the full design load.
- The bearing shall be designed to resist the full design moment.
- The bearing shall be designed to resist the full design shear.



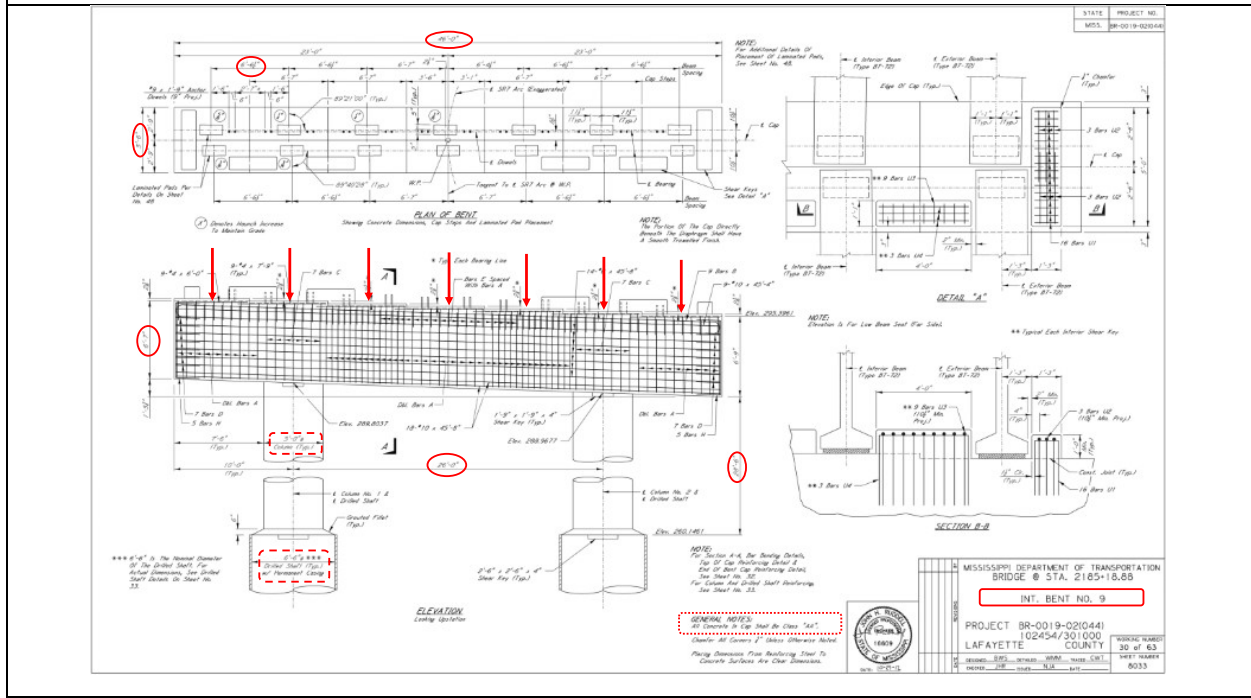
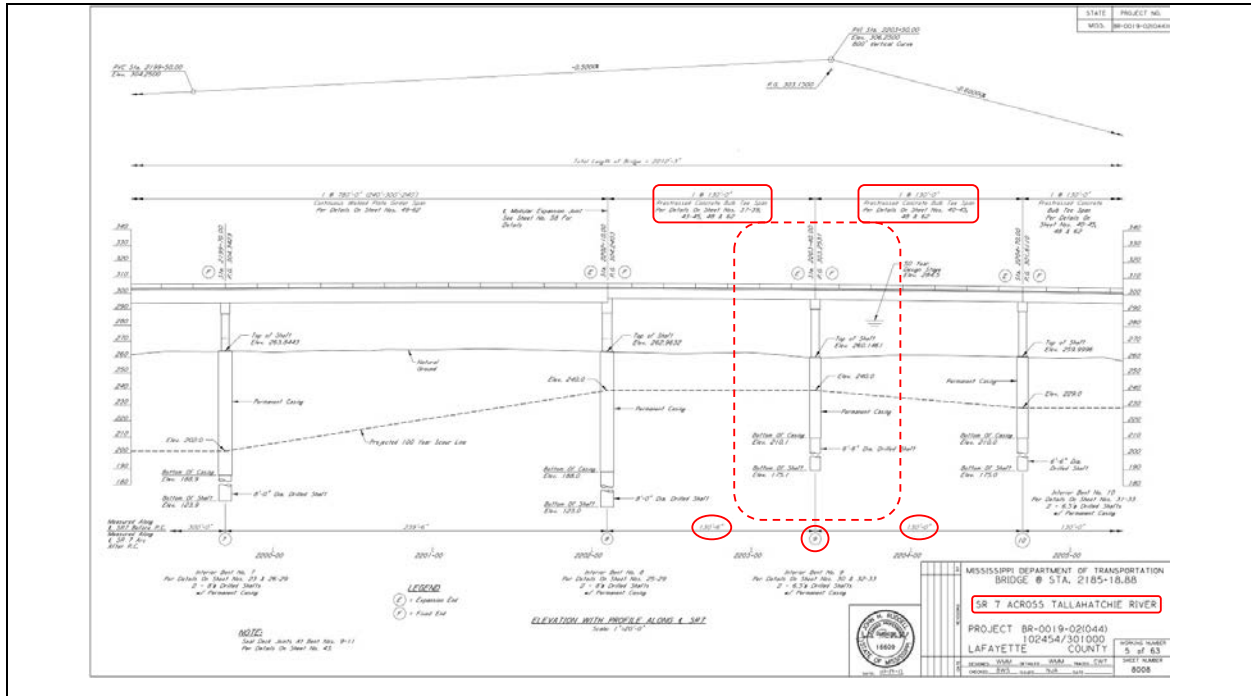
MISSISSIPPI DEPARTMENT OF TRANSPORTATION  
 BRIDGE # STA. 2185+18.88

PROJECT BR-019-020(44)  
 102454/301000  
 LAFAYETTE COUNTY

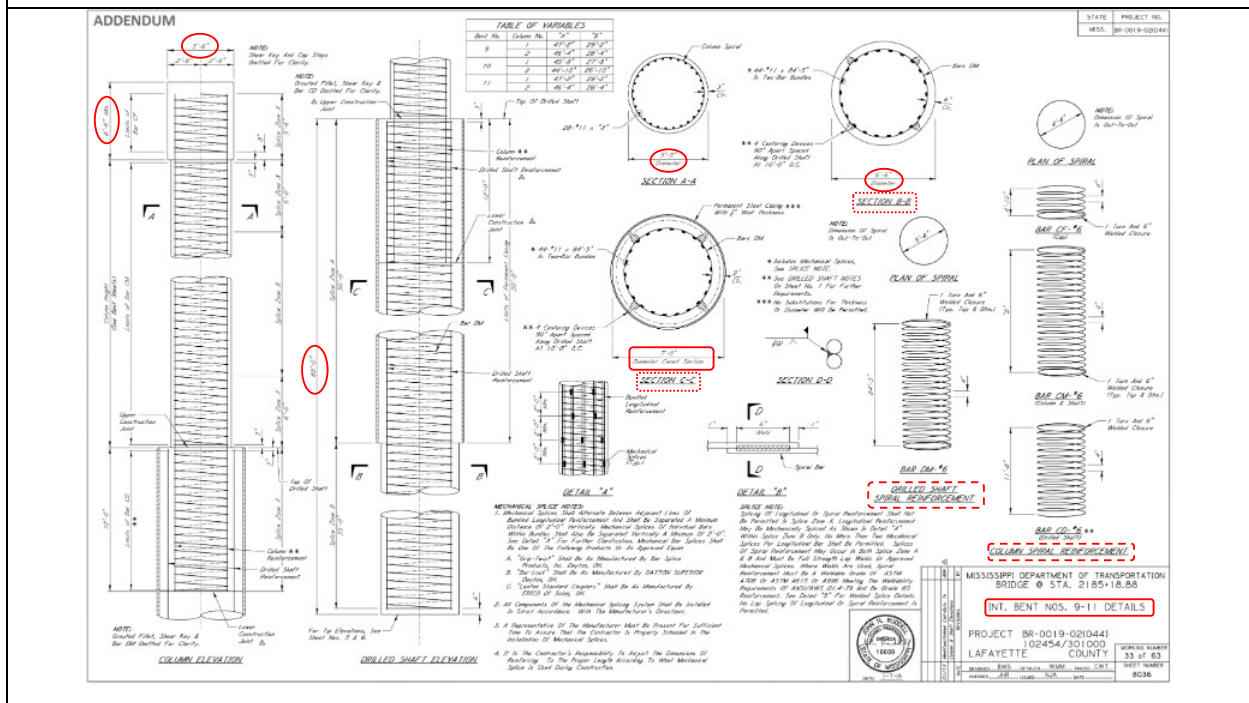
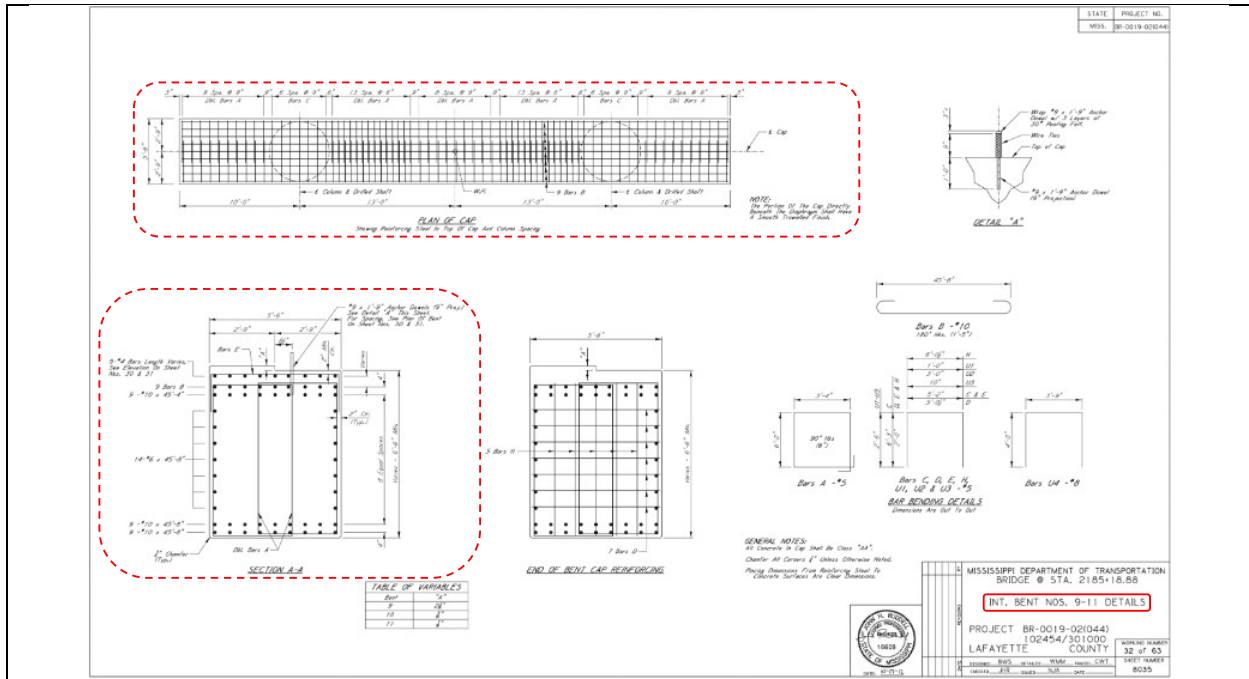
MISSISSIPPI DEPARTMENT OF TRANSPORTATION  
 BRIDGE # STA. 2185+18.88

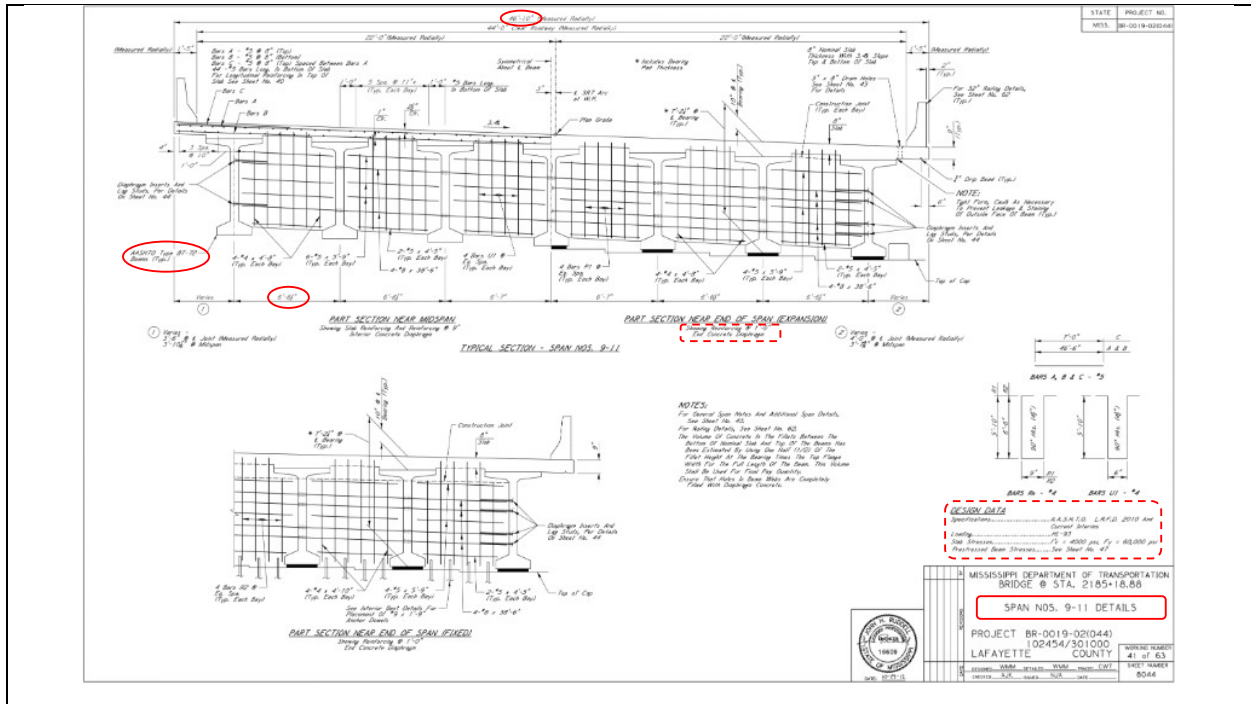
PROJECT BR-019-020(44)  
 102454/301000  
 LAFAYETTE COUNTY

# MS7 Substructure for Simple Spans with PC Bulb-Tee Girders (including Bent 9)









# US51 Substructure for Simple Spans with PC FIB Girders (including Bent 5)

**2nd O.REV.**

**GENERAL NOTES:**

1. Bridge Design Specifications for Steel and Bridge Construction, 2017 Edition, shall apply to all bridge components, unless otherwise specified.

2. The design of the bridge shall be in accordance with the design criteria set forth in the Bridge Design Specifications, 2017 Edition, unless otherwise specified.

3. The design of the bridge shall be in accordance with the design criteria set forth in the Bridge Design Specifications, 2017 Edition, unless otherwise specified.

4. The design of the bridge shall be in accordance with the design criteria set forth in the Bridge Design Specifications, 2017 Edition, unless otherwise specified.

5. The design of the bridge shall be in accordance with the design criteria set forth in the Bridge Design Specifications, 2017 Edition, unless otherwise specified.

6. The design of the bridge shall be in accordance with the design criteria set forth in the Bridge Design Specifications, 2017 Edition, unless otherwise specified.

7. The design of the bridge shall be in accordance with the design criteria set forth in the Bridge Design Specifications, 2017 Edition, unless otherwise specified.

8. The design of the bridge shall be in accordance with the design criteria set forth in the Bridge Design Specifications, 2017 Edition, unless otherwise specified.

9. The design of the bridge shall be in accordance with the design criteria set forth in the Bridge Design Specifications, 2017 Edition, unless otherwise specified.

10. The design of the bridge shall be in accordance with the design criteria set forth in the Bridge Design Specifications, 2017 Edition, unless otherwise specified.

**STEEL JOIST JOLE NOTES:**

1. Steel joist shall be driven with an approved metal hammer on a production job at the location shown in the MSJ TEST FILE SCHEDULE and will be paid for on test job only.

2. All steel joist shall be driven with an approved metal hammer on a production job at the location shown in the MSJ TEST FILE SCHEDULE, unless otherwise specified by the Director of Structures, State Bridge Engineer.

3. Approved joist shall be driven to an elevation no higher than the elevation shown in the REQUIRED JOLE BEARING CAPACITY AND JOLE ELEVATION SCHEDULE.

4. The Director of Structures, State Bridge Engineer may authorize that other drives include the structural steel.

5. After joist bearing pile shall be driven full length and be grouted with an approved by the Director of Structures.

6. After joist bearing pile shall be driven full length and be grouted with an approved by the Director of Structures.

7. After joist bearing pile shall be driven full length and be grouted with an approved by the Director of Structures.

8. After joist bearing pile shall be driven full length and be grouted with an approved by the Director of Structures.

9. After joist bearing pile shall be driven full length and be grouted with an approved by the Director of Structures.

10. After joist bearing pile shall be driven full length and be grouted with an approved by the Director of Structures.

Bent No.	Minimum Bearing Capacity (kips)	Steel Pipe	Minimum Top Elevation
1	240	24"	250.0
2	240	24"	250.0
3	240	24"	250.0
4	240	24"	250.0
5	240	24"	250.0
6	240	24"	250.0
7	240	24"	250.0
8	240	24"	250.0
9	240	24"	250.0

**ESTIMATED QUANTITIES**

Item	Quantity	Unit	Price	Total
1.00	1.00	cu yd	1.00	1.00
2.00	1.00	cu yd	1.00	1.00
3.00	1.00	cu yd	1.00	1.00
4.00	1.00	cu yd	1.00	1.00
5.00	1.00	cu yd	1.00	1.00
6.00	1.00	cu yd	1.00	1.00
7.00	1.00	cu yd	1.00	1.00
8.00	1.00	cu yd	1.00	1.00
9.00	1.00	cu yd	1.00	1.00
10.00	1.00	cu yd	1.00	1.00

**PILE SPACING DETAILS**

MISSISSIPPI DEPARTMENT OF TRANSPORTATION  
BRIDGE AT STA. 1518+76.92

**GENERAL NOTES - A**  
**ESTIMATED QUANTITIES**

PROJECT NUMBER BR-2401-2020-03  
COUNTY: PANOLA  
DATE: 03/11/2021

**DESIGN DATA:**

Specifications: AASHTO, LRFD BR. Edition, 2017 with 2018 Interim

Loadings: HS20, 100 ft. simple span

Clearance: 14'-0" over the water

Design speed: 55 mph

Structure: Steel girder

Structure type: Simple span

Structure material: Steel

**ELEVATION WITH PROFILE ALONG & APPROACH ROADWAY**

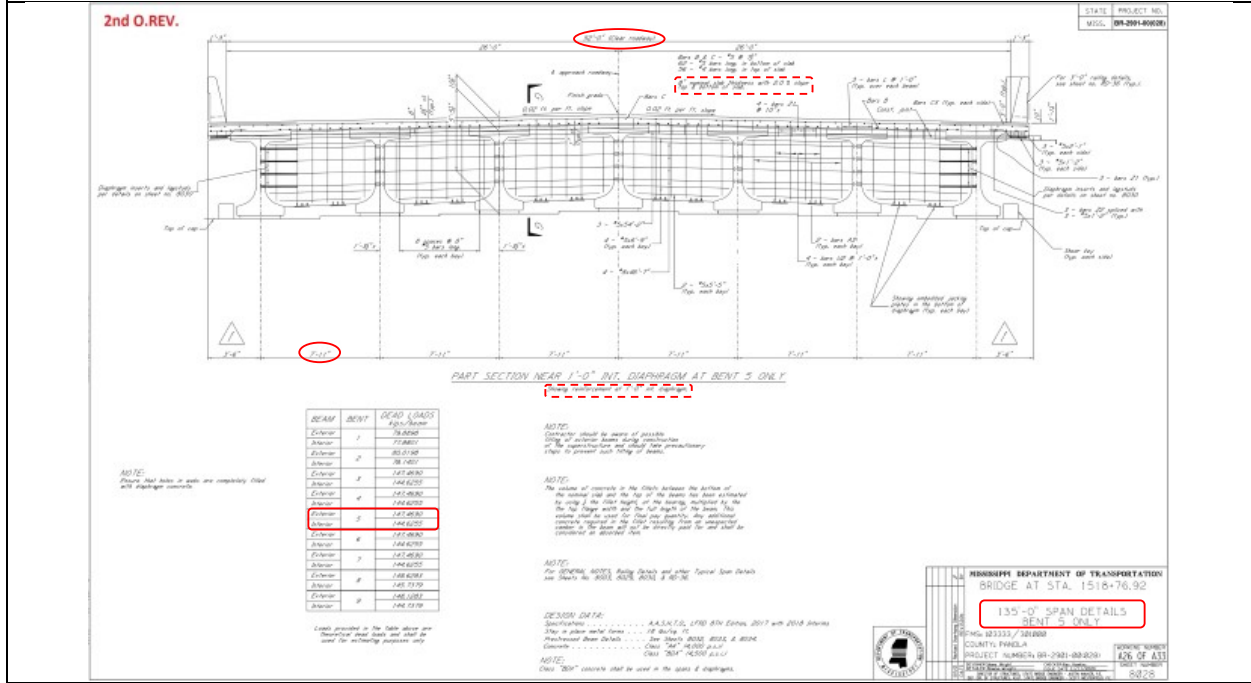
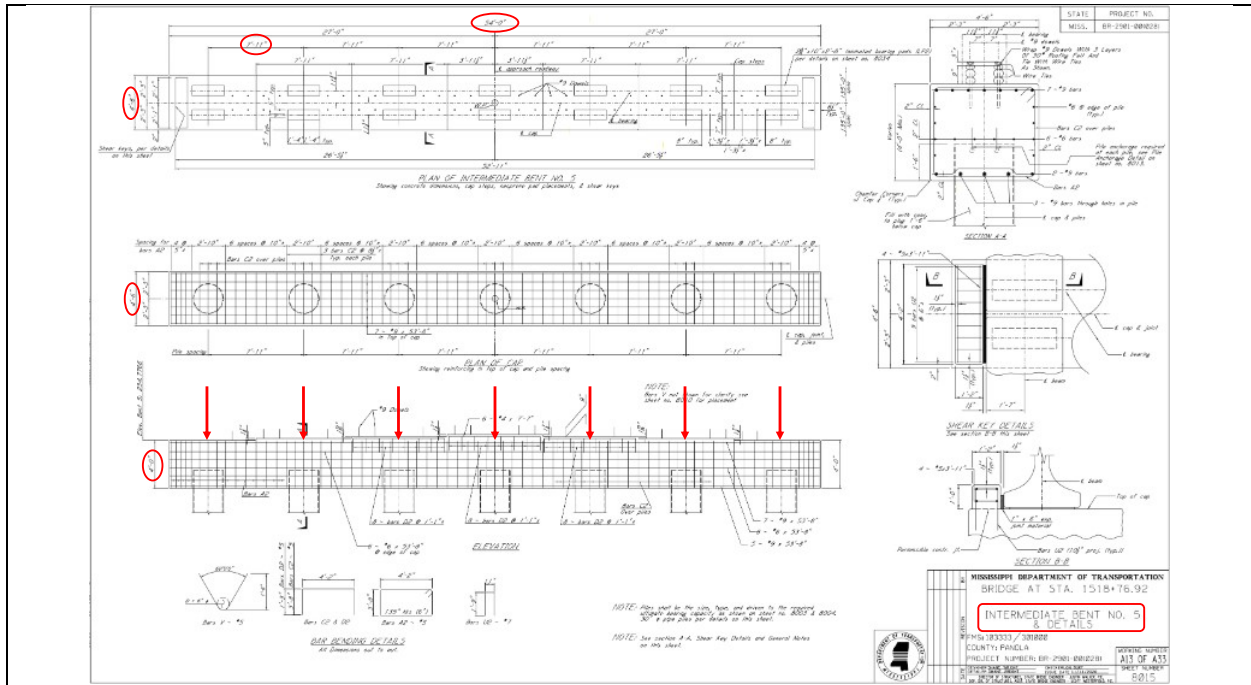
**DRAINAGE DATA:**

Item	Value
Channel width	62.5 ft.
Channel depth	2.0 ft.
Channel slope	2.0 ft./100 ft.
Channel material	Gravel

**MISSISSIPPI DEPARTMENT OF TRANSPORTATION**  
BRIDGE AT STA. 1518+76.92

**US HWY 51 OVER LONG CREEK LAYOUT**

PROJECT NUMBER BR-2401-2020-03  
COUNTY: PANOLA  
DATE: 03/11/2021

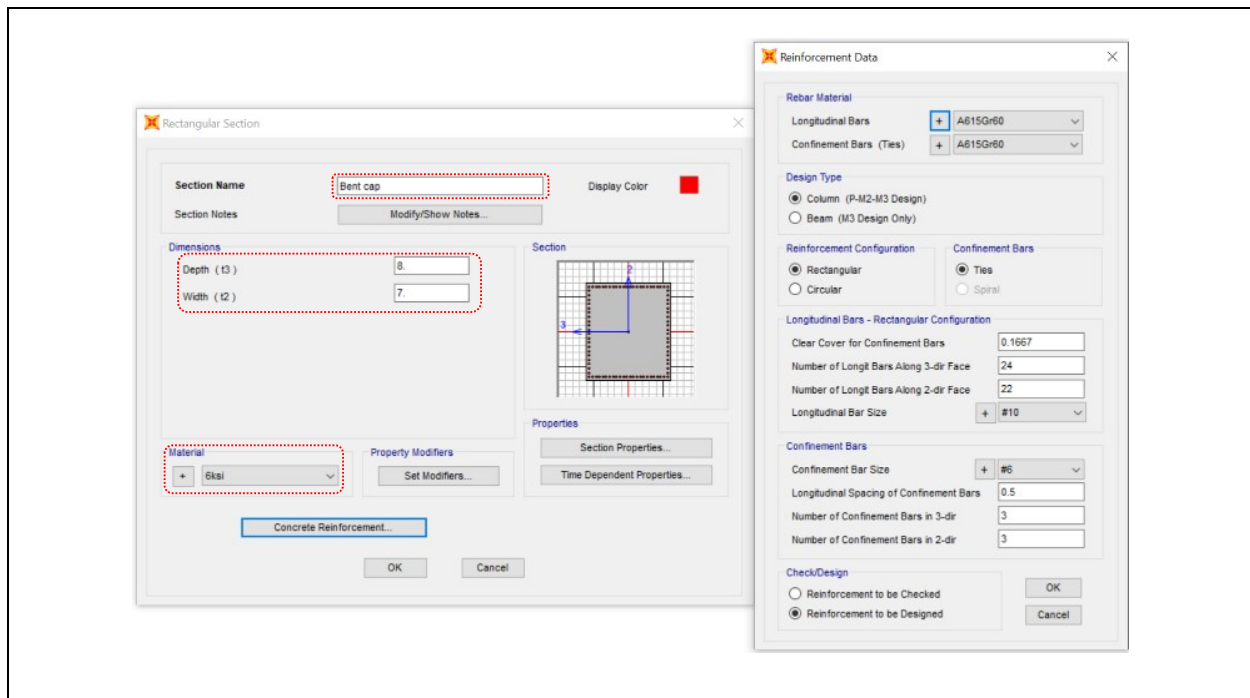


## Appendix C FE Software Descriptions and Menu Screen Captures

### SAP2000 Modeling and Screen Captures

The features of the SAP2000 modeling adopted in this study are found by searching links accessible using the *Help* tab provided with the software. These include *Contents*, *Index*, and *Search* tabs, and searchable *Documentation* and *CSI on the Web* links. The latter directs the user to the Computers and Structures, Inc., website technical support page where a searchable *Knowledge Base* and *Watch and Learn* resources are available as well as Reference Manuals and Tech Notes, <https://wiki.csiamerica.com/display/doc/Manuals> .

For clarity, select screen captures are provided below that provide modeling details as entered into the software for key features such as section and inelastic hinge definitions.

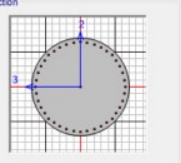


**Circle Section**

Section Name:  Display Color: ■

Section Notes:

Dimensions: Diameter (13):

Section: 

Material:  Property Modifiers:

**Reinforcement Data**

Rebar Material: Longitudinal Bars:  Confinement Bars (Ties):

Design Type:  Column (P-M2-M3 Design)  Beam (M3 Design Only)

Reinforcement Configuration:  Rectangular  Circular  Spiral

Confinement Bars:  Ties  Spiral

Longitudinal Bars - Circular Configuration: Clear Cover for Confinement Bars:  Number of Longitudinal Bars:  Longitudinal Bar Size:

Confinement Bars: Confinement Bar Size:  Longitudinal Spacing of Confinement Bars:

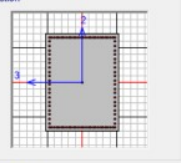
Check/Design:  Reinforcement to be Checked  Reinforcement to be Designed

**Rectangular Section**

Section Name:  Display Color: ■

Section Notes:

Dimensions: Depth (13):  Width (12):

Section: 

Material:  Property Modifiers:

**Reinforcement Data**

Rebar Material: Longitudinal Bars:  Confinement Bars (Ties):

Design Type:  Column (P-M2-M3 Design)  Beam (M3 Design Only)

Reinforcement Configuration:  Rectangular  Circular  Spiral

Confinement Bars:  Ties  Spiral

Longitudinal Bars - Rectangular Configuration: Clear Cover for Confinement Bars:  Number of Longit Bars Along 3-dir Face:  Number of Longit Bars Along 2-dir Face:  Longitudinal Bar Size:

Confinement Bars: Confinement Bar Size:  Longitudinal Spacing of Confinement Bars:  Number of Confinement Bars in 3-dir:  Number of Confinement Bars in 2-dir:

Check/Design:  Reinforcement to be Checked  Reinforcement to be Designed

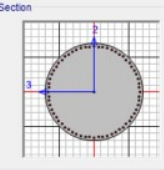


**Circle Section**

Section Name:  Display Color: ■

Section Notes:

Dimensions: Diameter (t3):

Section: 

Material:

**Reinforcement Data**

Rebar Material: Longitudinal Bars:  Confinement Bars (Ties):

Design Type:  Column (P-M2-M3 Design)  Beam (M3 Design Only)

Reinforcement Configuration:  Rectangular  Circular Confinement Bars:  Ties  Spiral

Longitudinal Bars - Circular Configuration: Clear Cover for Confinement Bars:  Number of Longitudinal Bars:  Longitudinal Bar Size:

Confinement Bars: Confinement Bar Size:  Longitudinal Spacing of Confinement Bars:

Check/Design:  Reinforcement to be Checked  Reinforcement to be Designed

**Link/Support Property Data**

Link/Support Type:  P-Delta Parameters:  Shear Couple  Equal End Moments  Advanced

Property Name:

Property Notes:

Total Mass and Weight: Mass:  Rotational Inertia 1:  Weight:  Rotational Inertia 2:  Rotational Inertia 3:

Factors For Line, Area and Solid Springs: Property is Defined for This Length in a Line Spring:  Property is Defined for This Area in Area and Solid Springs:

Directional Properties:

Direction	Fixed	NonLinear	Properties	Direction	Fixed	NonLinear	Properties
<input checked="" type="checkbox"/> U1	<input type="checkbox"/>	<input type="checkbox"/>	<input type="button" value="Modify/Show for U1..."/>	<input type="checkbox"/> R1	<input type="checkbox"/>	<input type="checkbox"/>	<input type="button" value="Modify/Show for R1..."/>
<input type="checkbox"/> U2	<input type="checkbox"/>	<input type="checkbox"/>	<input type="button" value="Modify/Show for U2..."/>	<input type="checkbox"/> R2	<input type="checkbox"/>	<input type="checkbox"/>	<input type="button" value="Modify/Show for R2..."/>
<input type="checkbox"/> U3	<input type="checkbox"/>	<input type="checkbox"/>	<input type="button" value="Modify/Show for U3..."/>	<input type="checkbox"/> R3	<input type="checkbox"/>	<input type="checkbox"/>	<input type="button" value="Modify/Show for R3..."/>

Stiffness Options: Stiffness Used for Linear and Modal Load Cases:  Stiffness Used for Stiffness-proportional Viscous Damping:  Stiffness-proportional Viscous Damping Coefficient Modification Factor:

**Link/Support Directional Properties**

Identification: Property Name:  Direction:  Type:  NonLinear:

Properties Used For All Analysis Cases: Effective Stiffness:  Effective Damping:

### Frame Hinge Property Data

**Hinge Property Name**  
FH1

**Hinge Type**  
 Force Controlled (Brittle)  
 Deformation Controlled (Ductile)  
 Interacting P-M3

Modify/Show Hinge Property...

OK Cancel

---

### Frame Hinge Property Data for FH1 - Interacting P-M3

**Hinge Specification Type**  
 Moment - Rotation  
 Moment - Curvature  
 Hinge Length:   
 Relative Length

**Scale Factor for Rotation (SF)**  
 SF is Yield Rotation per ASCE 41-13 Eqn. 9-2 (Steel Objects Only)  
 User SF:

**Load Carrying Capacity Beyond Point E**  
 Drops To Zero  Extrapolated

**Symmetry Condition**  
 Moment Rotation Dependence is Symmetric  
 Moment Rotation Dependence is Not Symmetric

**Requirements for Specified Symmetry Condition**  
 1 Specify curve at angle of 90°.

**Axial Forces for Moment Rotation Curves**  
 Number of Axial Forces:   
 Modify/Show Axial Force Values...

**Curve Angles for Moment Rotation Curves**  
 Number of Angles:   
 Modify/Show Angles...

Modify/Show Moment Rotation Curve Data...  
 Modify/Show P-M3 Interaction Surface Data...

OK Cancel

### Moment Rotation Data for FH1 - Interacting P-M3

Edit

Select Curve  
 Axial Force:  Angle:  Curve #1:  Units:

**Moment Rotation Data for Selected Curve**

Point	Moment/Yield Mom	Rotation/SF
A	0.	0.
B	1.	0.
C	1.1	0.015
D	0.2	0.015
E	0.2	0.025

Copy Curve Data Paste Curve Data

**Acceptance Criteria (Plastic Deformation / SF)**  
 Immediate Occupancy:   
 Life Safety:   
 Collapse Prevention:   
 Show Acceptance Points on Current Curve

**Moment Rotation Information**  
 Symmetry Condition:   
 Number of Axial Force Values:   
 Number of Angles:   
 Total Number of Curves:

**Angle is Moment About**  
 0 degrees = About Positive M2 Axis  
 90 degrees = About Positive M3 Axis  
 180 degrees = About Negative M2 Axis  
 270 degrees = About Negative M3 Axis

3D View: Plan  Elevation  Aperture   
 Hide Backbone Lines  Show Acceptance Criteria  Show Thickened Lines  Highlight Current Curve

OK Cancel

### Hinge Interaction Surface for FH1 - Interacting P-M3

**Interaction Surface Options**  
 Default from Material Property of Associated Line Object  
 Steel, AISI-LRFD Equations H1-1a and H1-1b with phi = 1  
 Steel, ASCE 41-13 Equation 9-4  
 Concrete, ACI 318-02 with phi = 1  
 User Definition  
 Define/Show User Interaction Surface...

**Axial Load - Displacement Relationship**  
 Proportional to Moment - Rotation  
 Elastic - Perfectly Plastic

OK Cancel

### Mass Source Data

Mass Source Name:

**Mass Source**  
 Element Self Mass and Additional Mass  
 Specified Load Patterns

**Mass Multipliers for Load Patterns**

Load Pattern	Multiplier
DEAD	1

Add Modify Delete

OK Cancel

### Load Case Data - Modal

Load Case Name:  Set Def Name Modify/Show...

**Stiffness to Use**  
 Zero Initial Conditions - Unstressed State  
 Stiffness at End of Nonlinear Case  
 Important Note: Loads from the Nonlinear Case are NOT included in the current case

**Number of Modes**  
 Maximum Number of Modes:   
 Minimum Number of Modes:

**Loads Applied**  
 Show Advanced Load Parameters

**Other Parameters**  
 Frequency Shift (Center):   
 Cutoff Frequency (Radius):   
 Convergence Tolerance:   
 Allow Automatic Frequency Shifting

**Load Case Type**  
 Modal Design...  
**Type of Modes**  
 Eigen Vectors  
 RTZ Vectors  
**Mass Source**

OK Cancel



**Time History - Function Definition**

**Function Name** EQ

**Function File**

File Name   
 c:\users\sgupta2\desktop\research\goodman m=8

Header Lines to Skip   
 Prefix Characters per Line to Skip   
 Number of Points per Line

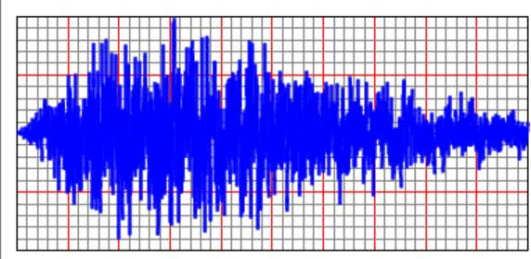
**Values are:**

Time and Function Values  
 Values at Equal Intervals of

**Format Type**

Free Format  
 Fixed Format  
 Characters per Item

**Function Graph**



**Load Case Data - Linear Modal History**

**Load Case Name** EQ

**Initial Conditions**

Zero Initial Conditions - Start from Unstressed State  
 Continue from State at End of Modal History

Important Note: Loads from this previous case are included in the current case

**Modal Load Case**

Use Modes from Case MODAL

**Loads Applied**

Load Type	Load Name	Function	Scale Factor
Accel	U1	EQ	48.9
Accel	U1	EQ	48.9

Show Advanced Load Parameters

**Time Step Data**

Number of Output Time Steps   
 Output Time Step Size

**Other Parameters**

Modal Damping

**Load Case Type** Time History

**Analysis Type**

Linear  
 Nonlinear

**History Type**

Transient  
 Periodic

**Solution Type**

Modal  
 Direct Integration  
 Frequency Domain

**Mass Source**

Previous (DECK)